

Supporting information for

Extension of the π -conjugated core of methylchalcogenolated polycyclic aromatic hydrocarbon: synthesis and characterization of 1,4,7,10-tetrakis(methylthio)- and tetramethoxy-coronene

Prasanta Pal,^{a,b†} Kirill Bulgarevich,^{a†} Ryota Hanaki,^c Kohsuke Kawabata^{a,c}, Kazuo Takimiya,^{a,b,c*}

^a RIKEN Center for Emergent Matter Science (CEMS), 2-1 Hirosawa, Wako, Saitama 351-0198, Japan

^b Tohoku University Advanced Institute for Materials Research (AIMR), 2-1-1 Katahira, Aoba-ku, Sendai, Miyagi 980-8577 Japan

^c Department of Chemistry, Graduate School of Science, Tohoku University, 6-3 Aoba, Aramaki, Aoba-ku, Sendai, Miyagi 980-8578 Japan

† P. P. and K. B. contributed equally.

1. Simulation of crystal structures of MT-coronene	S2
2. Synthesis and characterization	S5
3. Theoretical calculations	S13
4. Single-crystal X-ray analysis	S14
5. Photoemission yield spectroscopy	S17
6. Out-of-plane XRD	S17
7. Crystal structures of 5 and 12	S17
8. Crystal structures of methylthiolated naphthalene and perylene	S19
9. Single-crystal field-effect transistors (SC-FETs)	S19
10. Intermolecular overlap area	S20
11. NMR spectra	S21
12. High-resolution MS spectra	S30
13. APCI-MS and ¹H NMR spectra of crude MT-coronene	S32
14. References	S33

1. Simulation of crystal structures of MT-coronene and MO-coronene

The simulations of crystal structures of MT- and MO-coronene were carried out by following “*in silico* crystallization (ISC)” procedure reported.^{1,2} The method is based on systematic grid-based optimization of intermolecular arrangements and energetic evaluation using quantum chemical calculations. The bimolecular intermolecular interaction energies were calculated by using the Gaussian 16 program at B3lyp/6-31g(d,p) level.³ After constructing initial π -stacking dimers, two types of stacking searches were employed: (i) two-molecular stacking (2M), in which the central molecule and its two face-to-face neighbors were optimized simultaneously as a three molecular cluster, and (ii) one-molecular stacking (1M), where only the interaction between two molecules was considered. For each of the π -stacking configurations, molecular clusters were expanded in both the side-to-side and end-to-end directions to build a full brickwork (BW) structure. Interlayer configurations were then generated and optimized with conditional branching. In the first branching, different interlocking motifs of the BW layers, namely “cleavable layers (CL)” and “zipped layers (ZL)” were generated. In the second branching, “inclined brickwork (iBW)” arrangements were constructed based on corresponding BW structures and vector algebra to define mirror and rotation operations on the BW layers, followed by further energy minimization of intermolecular contacts. Together, the combination of stacking mode (1M or 2M), interlayer packing (CL or ZL), and interlayer orientation (BW or iBW) generated eight distinct polymorph candidates (Table S1, Fig. S1).

The current ISC algorithm is designed exclusively to generate BW-related polymorph candidates. Therefore, the dimeric experimental structure of MO-coronene, which does not belong to the BW class, was not reproduced by ISC. However, the configuration of the experimental π -stacking dimer (related by vector (1.49, -0.31, 3.46) Å in Cartesian system) was reasonably close to the π -stacking configuration of the simulated 1M polymorphs (1.8, 0.0, 3.5) Å. This similarity likely reflects the dominance of π - π interactions in the overall packing structure; variations in the arrangement of surrounding molecules do not significantly disturb the preferred π -stacking motif from the position derived from the simplest bimolecular interaction assumption. This observation supports the core assumption of the ISC protocol: π -stacking geometry can be reasonably optimized based on local interactions alone without considering the other molecular surroundings.

As for the MT-coronene case, the BW structures that resemble the experimental structure were generated. Among them, the 1M-CL-BW polymorph candidate notably exhibits a similar zig-zag arrangement in the end-to-end direction, resembling the interlocking arrangement induced by the methylthio groups in the experimental structure. However, the x_1 and y_1 of the 1M ($x_1 = 1.8$, $y_1 = 0.0$ Å) and 2M ($x_1 = 5.3$, $y_1 = 0.0$ Å) polymorphs were both markedly different from that of the experimental BW structure ($x_1 = 3.62$, $y_1 = -1.47$ Å) Å (see Table S1). Notably, all simulated structures lacked a y -offset of the π -stacking configuration and appeared very promising in terms of intermolecular orbital overlap. On the other hand, a similar π -stacking configuration to MT-coronene with a large y -offset was previously simulated in the MT-perylene 2M-CL-BW polymorph in good agreement with the experimental structure of MT-perylene.

All four simulated 2M-polymorph candidates of MT-coronene, however, exhibited unusually large voids in the end-to-end direction, particularly between the methylthio groups. In contrast, these voids were effectively filled in the corresponding 2M polymorphs of MT-perylene. This discrepancy highlights a fundamental limitation of the current ISC algorithm: it does not incorporate any penalty or energy correction for the presence of voids or inefficient packing in the broader crystal structure. Since ISC optimizes crystal structures solely by minimizing pairwise interaction energies, it lacks a mechanism for evaluating the energetic penalty associated with unfilled space. For relatively large, rigid molecules like coronene, the energetic gain from maximizing π - π stacking interactions may outweigh the destabilization caused by packing inefficiencies, leading the algorithm to favor structures that do not correspond well to the experimentally observed, more densely packed arrangements. Incorporating a correction term that penalizes structural voids could therefore improve the predictive accuracy of ISC for larger π -conjugated systems.

Table S1 Displacements of the π -stacking molecules in simulated and experimental structures of MT- and MO-coronene.

Compound	Structure ^a	x_1 ^b	y_1 ^b	z_1 ^b	x_2 ^b	y_2 ^b	z_2 ^b	μ_{hop} ^c
MT-coronene	1M-CL-BW	1.80	0.00	3.57	-10.86	3.50	3.06	9.5
	1M-ZL-BW	1.80	0.00	3.57	-12.66	0.00	3.57	9.5
	2M-CL-BW	5.30	0.00	3.51	-8.96	0.20	3.66	16.0
	2M-ZL-BW	5.30	0.00	3.51	-8.96	0.00	3.66	15.9
	Experimental	3.62	-1.47	3.48	-9.10	2.36	3.46	0.5
MO-coronene	1M-CL-BW	1.80	0.00	3.49	-10.13	3.40	3.20	7.5
	1M-ZL-BW	1.80	0.00	3.49	-11.33	-0.20	3.80	7.5
	2M-CL-BW	5.30	0.70	3.50	-7.63	1.20	3.43	1.2
	2M-ZL-BW	5.30	-0.80	3.49	-7.53	-0.10	3.46	0.8
	Experimental	1.49 ^d	-0.31 ^d	3.46 ^d	- ^e	- ^e	- ^e	- ^e

^a 1M: one molecular stacking, 2M: two molecular stacking, CL: cleavable layers, ZL: zipped layers.

^b Å. ^c cm² V⁻¹ s⁻¹. ^d Vector between the π -stacking dimer. ^e Not defined for the dimeric structure.

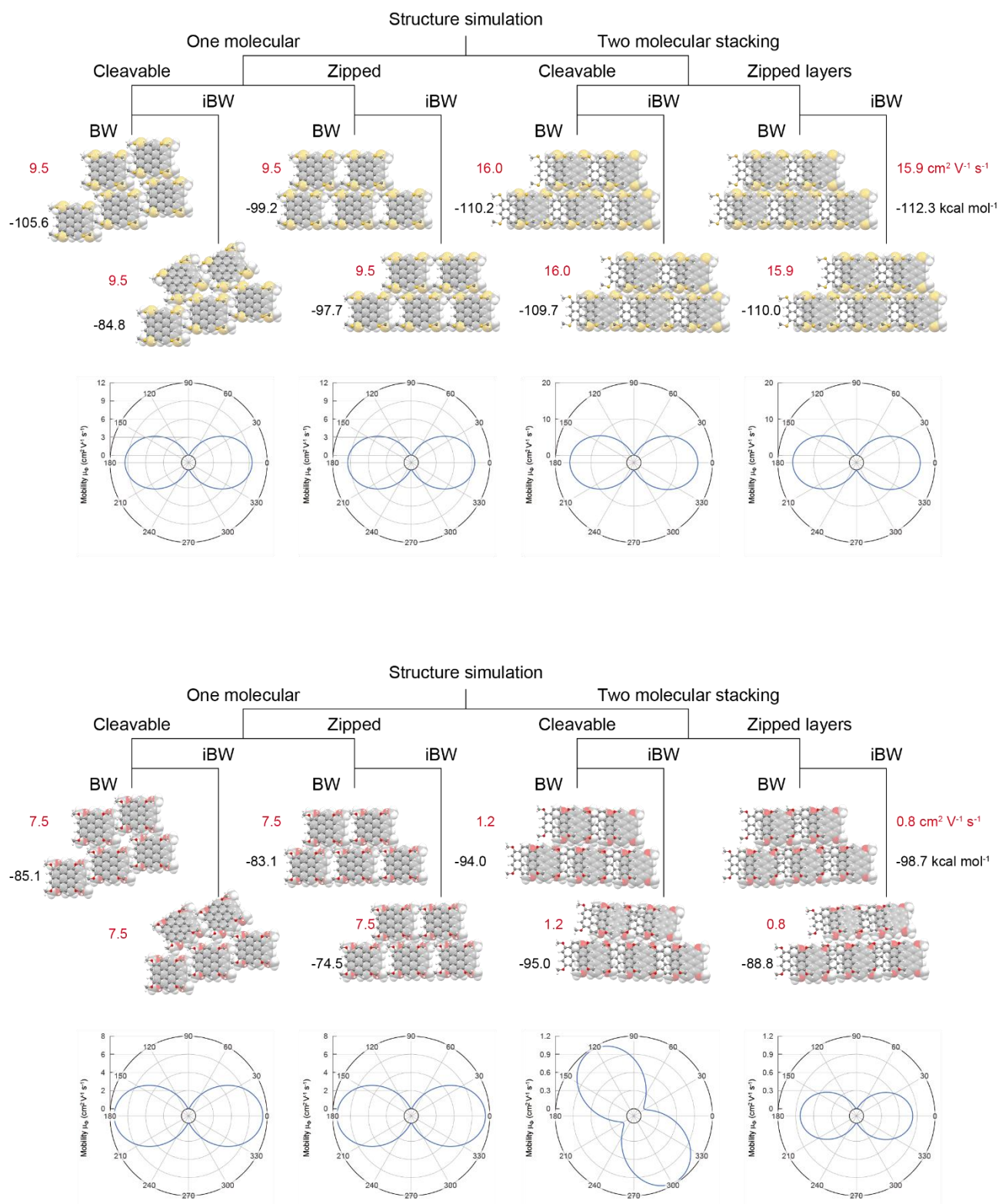
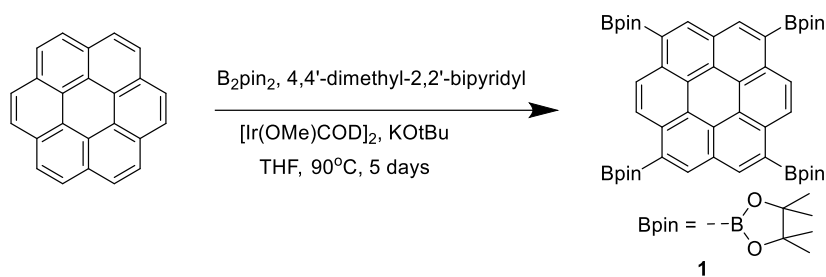


Fig. S1. Simulated crystal structures of MT-coronene (top) and MO-coronene (bottom): 8 brickwork-related polymorph candidates with simulated anisotropic mobilities (red values) and interaction energy sum of a molecule with 14 molecular surrounding molecules (black values). Note that simulated brickwork layers are identical between a brickwork and the corresponding inclined brickwork structure, resulting in identical anisotropic mobilities.

2. Synthesis and characterization

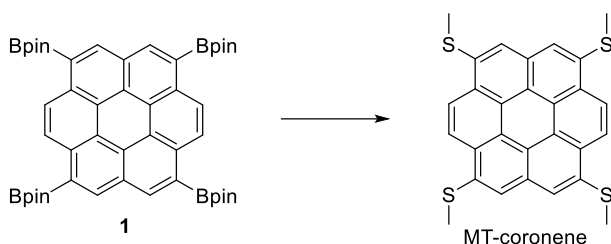
Materials and Instrumentations: All reagents and solvents used here were purchased from Tokyo Chemical Industry Co., Kanto Chemical Co., FUJIFILM Wako Pure Chemical Corporation or Sigma-Aldrich Co. and used without further purification unless otherwise noted. Coronene was purified by vacuum sublimation prior to use in the borylation reaction. Solvents used in the reactions were dried with a Glass Contour solvent purification system. ^1H NMR (400 MHz and 500 MHz) and ^{13}C NMR (101 MHz) spectra were recorded using a JEOL ECS-400 spectrometer at room temperature, with tetramethylsilane (TMS; 0 ppm) as the internal standard. High-resolution mass spectrometry was performed with a Bruker micrOTOF II mass spectrometer equipped with an atmospheric pressure chemical ionization source in APCI TOF-MS in dichloromethane solvent, and the Matrix-assisted laser desorption/ionization time-of-flight mass spectrometry (MALDI TOF-MS) was performed with a JEOL JMS-S3000, with dithranol as a matrix in tetrahydrofuran solvent.

*1,4,7,10-tetrakis(4,4,5,5-tetramethyl-1,3,2-dioxaborolan-2-yl)coronene*⁴



$[\text{Ir}(\text{OMe})\text{COD}]_2$ (106 mg, 0.16 mmol), 4,4'-di-tert-butyl-2,2'-bipyridyl (86 mg, 0.32 mmol), B_2pin_2 (1.4 g, 5.6 mmol), and KOtBu (10 mg, 0.08 mmol) were taken in a glass pressure vessel equipped with a magnetic stirring bar and a silicon rubber septum under nitrogen atmosphere. THF (1.5 mL) was added by syringe, and the mixture was heated at 50°C for 15 min. Coronene (240 mg, 0.80 mmol) was added, and the rubber septum was replaced with a pressure vessel cap. The reaction mixture was then continuously heated at 90°C in an oil bath for 5 days without interruption. The mixture was then cooled to room temperature, opened to the air, and diluted with dichloromethane (5 mL). The reaction was quenched by the dropwise addition of 10% aqueous HCl (3 mL). The mixture was then extracted with dichloromethane and water. The organic part was evaporated under reduced pressure, and then methanol was added. The resulting greenish-yellow precipitate was collected, which was mostly pure **1** (130 mg), and used for the next reaction. The remaining mixture was first separated using a silica gel column with hexane:ethyl acetate (9:1, v/v) as the eluent, and the crude product was collected. It was then purified by gel permeation chromatography (GPC) using CHCl_3 as the eluent. The GPC-separated tetra-borylated fraction was a mixture of regioisomers, which was washed with methanol to give **1** (overall yield ca. 30%). ^1H NMR (CDCl_3 , 400 MHz): δ (ppm) 9.89 (s, 4H), 9.59 (s, 4H), 1.61 (s, 48H).

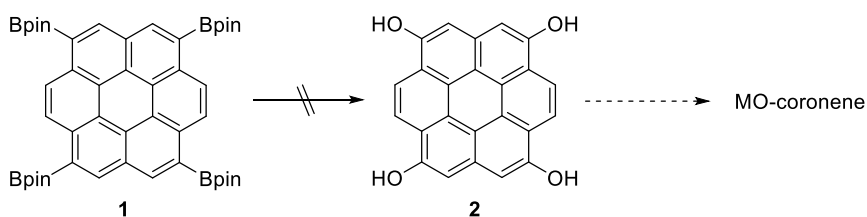
1,4,7,10-Tetrakis(methylthio)coronene (MT-coronene)



Copper(II) sulfate (80 mg, 0.50 mmol), cesium fluoride (840 g, 5.53 mmol), and *N,N,N',N'*-tetramethylethylenediamine (80 mg, 0.69 mmol) were added to a solution of methyl *p*-toluenethiosulfonate (800 mg, 3.96 mmol) and Bpin-Coronene (**1**, 400 mg, 0.50 mmol) dissolved in methanol (50 mL) at room temperature.⁵⁻⁷ The reaction mixture was refluxed for 24 h, and the resulting precipitate was washed several times with methanol and water, collected by filtration, and dried in air. The solid was continuously washed with boiling methanol and then extracted with boiling toluene. The insoluble part was collected and dried. The title compound was obtained after vacuum sublimation (more than three times) from the crude product as a yellow solid (up to 10%). Mp >300°C. ¹H NMR (1,1,2,2-Tetrachloroethane-*d*₂ (TCE-*d*₂) at 120 °C, 400 MHz, very poor solubility) δ (ppm) 9.41 (s, 4H), 8.80 (s, 4H), 2.97 (s, 12H). ¹³C NMR (CDCl₃, 100 MHz): δ (ppm) No peaks for very poor solubility. HRMS (MALDI-TOF) *m/z*: [M]⁺ Calcd for 484.0448, found 484.0433.

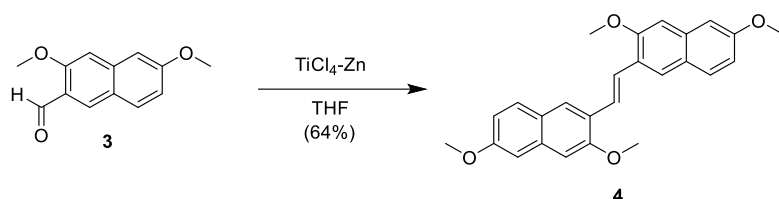
Note: From 400 mg of **1**, we obtained an average of 100 mg (ca. 40%) of insoluble crude product (exact amount varying batch to batch) after thorough workup of the reaction mixture prior to sublimation. The crude product contained mostly tetrakis- (MT-coronene) and tris-methylthiolated coronene, along with other byproducts (bismethylthiolated coronenes), as judged from the MS (APCI, not high-resolution) and ¹H NMR spectra (Fig. 30 and S31, respectively). These poorly soluble byproducts could not be separated by the normal workup measures, including chromatography and recrystallization. Thus, vacuum sublimation was applied to purify MT-coronene; however, the major byproduct, tris-methylthiolated coronene, was not completely separated by the first sublimation. Pure MT-coronene was only obtained after repetitive vacuum sublimations (source temperature: ca. 400 °C under 10⁻² Pa). The high source temperature always induced decomposition of the source material, which reduced the overall yield of pure MT-coronene. As the byproducts, including tris-methylthiolated coronene, have better solubility than that of MT-coronene, the ¹H NMR spectroscopy was the most reliable measure to ensure the purity of MT-coronene, as shown in Fig. S25.

Attempted Synthesis of MO-Coronene from 1



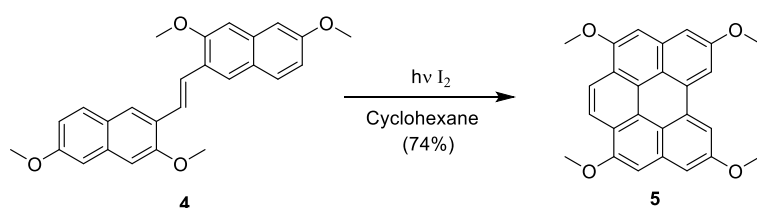
To a solution of **1** (100 mg, 0.124 mmol) in a degassed mixture of THF/acetone/H₂O (20 mL:2.5 mL:1.5 mL), Oxone (615 mg, 0.99 mmol) was added.⁸ The mixture was then stirred at room temperature overnight. A precipitate obtained (with no peaks corresponding to **2** in mass spectroscopy) was further used for the methylation reaction: a mixture of the precipitate, 250 mg of K₂CO₃, and 500 μL of CH₃I in *N,N*-dimethylformamide (DMF, 15 mL) was stirred 24 h at room temperature. A general workup was done, but MO-coronene was not detected by mass and ¹H NMR spectroscopy.

(E)-1,2-Bis(3,6-dimethoxynaphthalen-2-yl)ethene (4)



Under a nitrogen atmosphere, to a deaerated THF (150 mL) was added TiCl₄ (4.0 mL, 36 mmol) dropwise and Zinc (4.75g, 72 mmol) at 0 °C, After the mixture was stirred for 15 min at 0 °C. **3**⁹ (6.49 g, 30 mmol) was added to the mixture at 0 °C, and the resulting mixture was refluxed for 17 h.¹⁰ After cooling to room temperature, the mixture was poured into a sodium carbonate aqueous solution (150 mL). Dichloromethane (600 mL) was added, and then the mixture was stirred for 18 h at room temperature. The precipitate was separated by filtration and further washed thoroughly with dichloromethane (500 mL). The combined organic layer was washed with water and brine, dried (MgSO₄), and concentrated in vacuo to give a yellow solid. The crude product was purified by silica gel column chromatography, eluted with dichloromethane, and then recrystallized (toluene) to give **4** as a yellow solid (3.84 g, 64%), Mp 240–242 °C. ¹H NMR (CDCl₃, 400 MHz): δ (ppm) 8.02 (s, 2H), 7.71 (d, *J* = 8.9 Hz, 2H), 7.65 (s, 2H), 7.06 (s, 2H), 7.05 (d, *J* = 2.7 Hz, 2H), 7.02-6.99 (dd, *J* = 8.9, 2.7 Hz, 2H), 4.00 (s, 6H), 3.92 (s, 6H). ¹³C NMR (CDCl₃, 100 MHz): δ (ppm) 158.17, 156.34, 135.39, 129.40, 126.47, 125.53, 124.33, 124.25, 116.38, 104.96, 105.07, 55.58, 55.37. HRMS (MALDI-TOF) *m/z*: [M]⁺ Calcd. for 400.1675, found 400.1670, Anal. Calcd. for C₂₆H₂₄O₄: C, 77.98; H, 6.04%. Found: C, 77.63; H, 6.17%.

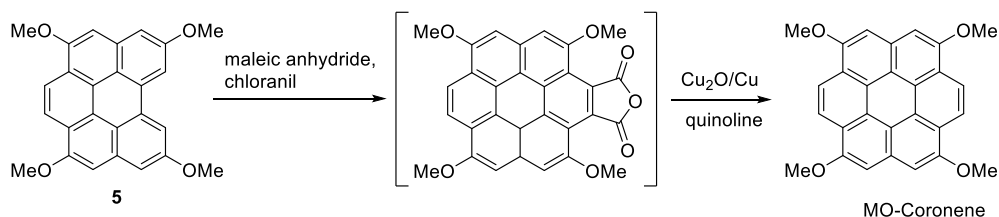
3,6,9,12-Tetramethoxybenzo[ghi]perylene (5)¹¹



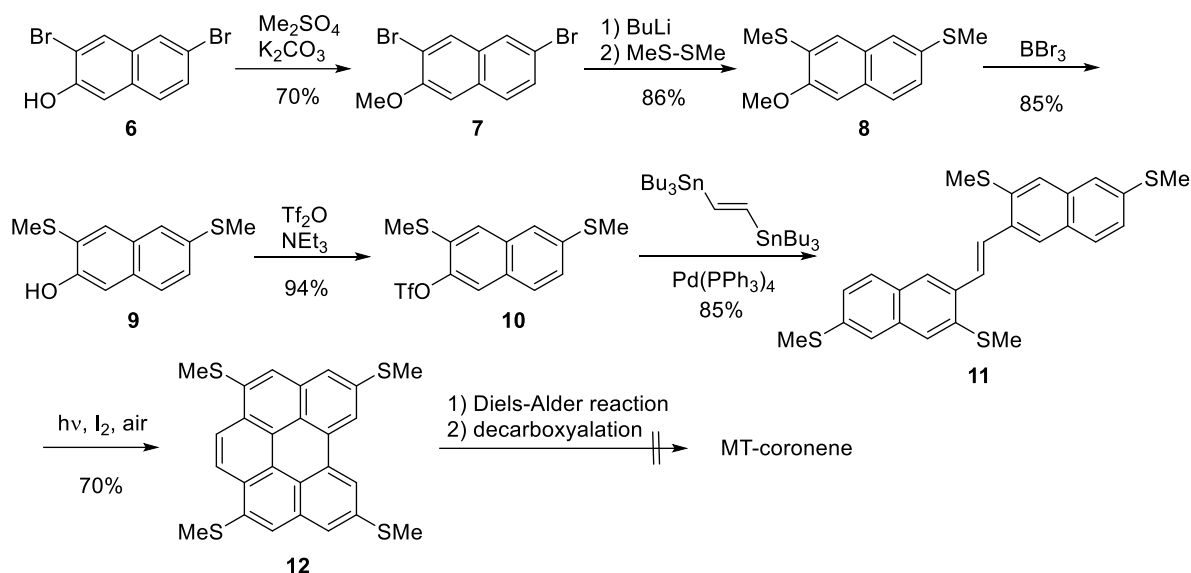
A solution of **4** (321 mg, 0.8 mmol) and iodine (32 mg, 0.25 mmol) in cyclohexane (500 mL) was irradiated with 27W black light for 13h under air. The solvent was evaporated, and the resulting solid was dissolved in chloroform (100 mL). The chloroform solution was successively washed with sodium thiosulfate aqueous solution and water, dried (MgSO₄), and concentrated in vacuo. The

crude product was purified by silica gel column chromatography (eluent: dichloromethane) and recrystallization (toluene) to give **5** as a yellow solid (236 mg, 74%). Mp > 400 °C. ¹H NMR (CDCl₃, 400 MHz) δ (ppm) 8.70 (s, 2H), 8.32 (d, *J* = 2.4 Hz, 2H), 7.58 (d, *J* = 2.4 Hz, 2H), 7.27 (s, 2H), 4.23 (s, 6H), 4.13 (s, 6H). ¹³C NMR (CDCl₃, 100 MHz): δ (ppm) 158.33, 155.07, 134.70, 131.33, 123.99, 122.84, 118.69, 117.21, 108.62, 106.74, 102.34, 55.67, 55.63. HRMS (MALDI-TOF) *m/z*: [M]⁺ Calcd. for C₂₆H₂₀O₄: 396.1362, found 396.1381, Anal. Calcd. for C₂₆H₂₀O₄: C, 78.77; H, 5.09%. Found: C, 78.60; H, 5.06%.

1,4,7,10-Tetramethoxycoronene (MO-coronene)¹²

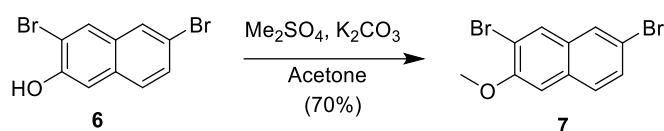


Under nitrogen atmosphere, **5** (201 mg, 0.51 mmol), *p*-chloranil (325 mg, 1.32 mmol) and maleic anhydride (3.0 g, 30 mmol) were heated 200 °C for 3 h. To the mixture, *p*-xylene (15 mL) was added and refluxed for 1h. After cooling, the mixture was diluted with ether (15 mL), and the resulting precipitate was collected by filtration. The filtrate was treated in a refluxing solvent (chloroform/ethyl acetate 1:2 v/v, 45 mL) to give 2,5,8,12-tetramethoxycoroneno[1,2-*c*]furan-9,11-dione as a purple solid (225 mg, 90%). Mp. > 400 °C. ¹H NMR (CDCl₃, 500 MHz) δ (ppm) 8.89 (s, 2H), 7.79 (s, 2H), 7.69 (s, 2H), 4.44 (s, 6H), 4.39 (s, 6H). IR: ν (cm⁻¹) 1841, 1823, 1805, 1784, 1760. The above product (243.2 mg, 0.5 mmol) was suspended in quinoline (50 mL), and Cu₂O (859 mg, 6 mmol) and Cu (78 mg, 1.2 mmol) were added to the suspension. The mixture was heated at 220 °C for 20 h, cooled to room temperature, and diluted with hydrochloric acid aqueous solution (10%, 150 mL). The precipitate collected by filtration was purified by silica-gel column chromatography, eluted with toluene to give MT-coronene as a yellow solid. An analytical sample was obtained by vacuum sublimation as a yellow solid (yield: 10–15% in two steps). Mp > 400 °C. ¹H NMR (CDCl₃, 400 MHz) δ (ppm) 9.07 (s, 4H), 8.06 (s, 4H), 4.42 (s, 12H). ¹³C NMR (CDCl₃, 100 MHz): no peak owing to very poor solubility. HRMS (MALDI-TOF) *m/z*: [M]⁺ Calcd for C₂₈H₂₀O₄: 420.1362, found 420.1365, Anal. Calcd for C₂₈H₂₀O₄: C, 79.98; H, 4.79%. Found: C, 79.73; H, 4.83%.



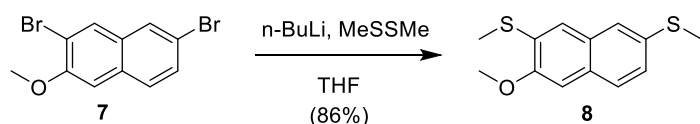
Scheme S1. Attempted synthesis of MT-coronene in a stepwise manner via benzo[*ghi*]perylene (**12**).

3,6-Dibromo-2-methoxynaphthalene (**7**)



A mixture of **6**¹³ (6.0 g, 20 mmol), K_2CO_3 (8.3 g, 60 mmol), and dimethyl sulfate (3.8 mL, 40 mmol) in acetone (100 mL) was stirred for 23 h at 80 °C, and the resulting precipitate was filtered off. The filtrate was concentrated, and the resulting solid was washed with water and dried *in vacuo*. The crude solid was dissolved in dichloromethane, washed with water, dried (MgSO_4), and concentrated *in vacuo*. The crude product was purified by flash silica gel column chromatography (eluent: dichloromethane) and reprecipitation with chloroform and hexane to give the title compound (**7**, 4.4 g, 70%) as a colorless solid. Mp 147.2–150.2 °C. ^1H NMR (CDCl_3 , 400 MHz) δ (ppm) 7.97 (s, 1H), 7.84 (s, 1H), 7.60–7.58 (d, $J = 8.7$ Hz, 1H), 7.53–7.51 (dd, $J = 8.7, 1.9$ Hz, 1H), 7.11 (s, 1H), 4.00 (s, 1H). ^{13}C NMR (CDCl_3 , 100 MHz): δ (ppm) 153.97, 132.07, 131.43, 130.42, 130.11, 128.74, 128.34, 118.11, 114.73, 106.60, 56.37. HRMS (APCI) m/z : $[\text{M}]^+$ Calcd for $\text{C}_{11}\text{H}_8\text{Br}_2\text{O}$: 315.8921, found 315.8912.

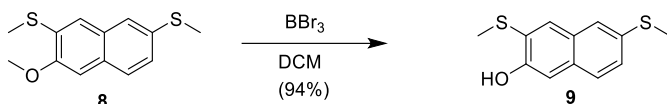
2,7-Bis(methylthio)-3-methoxynaphthalen (**8**)



Under a nitrogen atmosphere, to a solution of **7** (1.58 g, 5 mmol) in THF (20 mL) was added $n\text{-BuLi}$ (2.66 M hexane solution, 4.5 mL, 12 mmol) and dimethyl disulfide (1.8 mL, 20 mmol) dropwise at -80 °C. After the mixture was warmed to r.t for 5 h. The mixture was quenched with water and extracted with dichloromethane. The organic extract was washed with water and brine, dried over

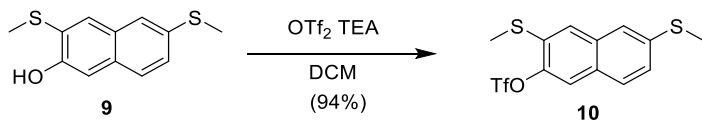
anhydrous MgSO_4 , and concentrated in vacuo. The crude product was subjected to column chromatography on silica gel eluting with dichloromethane-hexane (7:3 v/v) to give the title compound (**8**, 7.1 g, 86%) as a pale-yellow solid. Mp 96.1–98.2 °C. ^1H NMR (CDCl_3 , 400 MHz) δ (ppm) 7.62–7.60 (d, $J = 8.6$ Hz, 1H), 7.52 (s, 1H), 7.36 (s, 1H), 7.32–7.29 (dd, $J = 8.7, 1.9$ Hz, 1H), 7.03 (s, 1H), 3.99 (s, 3H), 2.57 (s, 3H), 2.54 (s, 3H). ^{13}C NMR (CDCl_3 , 100 MHz): δ (ppm) 154.24, 133.76, 130.59, 129.98, 129.81, 126.96, 125.54, 123.05, 122.01, 104.76, 55.99, 16.39, 14.54. HRMS (APCI) m/z : $[\text{M}]^+$ Calcd for $\text{C}_{13}\text{H}_{14}\text{OS}_2$: 250.0486, found 250.0472.

3,6-Bis(methylthio)naphthalen-2-ol (**9**)



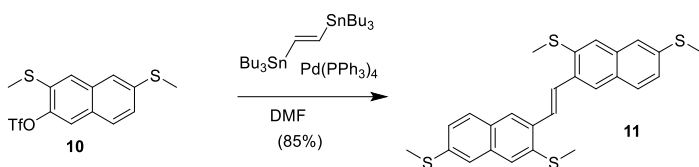
Under a nitrogen atmosphere, a solution of boron tribromide (BBr_3) in dichloroethane (ca. 1 M, 30 mmol) was added to a solution of **8** (2.50 g, 10 mmol) in dichloroethane (50 mL) at 0 °C, and the resulting mixture was stirred for 1 h at 0 °C. The mixture was poured into ice-cooled water (approximately 100 mL) at 0 °C and was extracted with dichloromethane three times. The combined organic layer was washed with brine, dried (MgSO_4), and concentrated in vacuo. The residue was subjected to silica-gel column chromatography, eluted with dichloromethane. The crude product was further purified by reprecipitation from chloroform/hexane to give the title compound (**9**, 2.23 g, 94%) as a colorless solid. Mp 132.7–136.8 °C. ^1H NMR (CDCl_3 , 400 MHz) δ (ppm) 7.90 (s, 1H), 7.61–7.59 (d, $J = 8.7$ Hz, 1H), 7.52 (s, 1H), 7.36–7.33 (dd, $J = 8.7, 1.9$ Hz, 1H), 7.27 (s, 1H), 6.55 (s, 1H), 2.56 (s, 3H), 2.43 (s, 3H). ^{13}C NMR (CDCl_3 , 100 MHz): δ (ppm) 152.42, 133.68, 132.98, 132.76, 129.49, 127.30, 126.93, 125.12, 123.59, 109.38, 19.83, 16.31. HRMS (APCI) m/z : $[\text{M}]^+$ Calcd for $\text{C}_{12}\text{H}_{12}\text{OS}_2$: 236.0330, found 236.0329.

3,6-Bis(methylthio)naphthalen-2-yl trifluoromethanesulfonate (**10**)¹¹



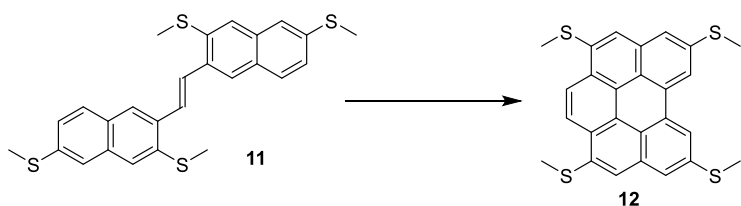
To a solution of **9** (3.54 g, 15 mmol) and triethylamine (5.2 mL, 37.5 mmol) in dichloromethane (150 mL) was dropwise added trifluoromethane sulfonic anhydride (3.3 mL, 19.5 mmol) at 0 °C, and the resulting mixture was stirred for 1h at the same temperature. The reaction mixture was diluted with water (300 mL) and extracted with dichloromethane. The extract was washed with water and brine and dried (MgSO_4). The crude product was purified by silica-gel column chromatography (eluent: dichloromethane: hexane, 1:3 v/v) to give the title compound (**10**, 5.42 g, 98%) as a white solid. Mp 68.2–71 °C. ^1H NMR (CDCl_3 , 400 MHz) δ (ppm) 7.69–7.67 (d, $J = 8.7$ Hz, 1H), 7.65 (s, 1H), 7.55 (s, 1H), 7.50 (s, 1H), 7.38–7.36 (dd, $J = 8.7, 1.9$ Hz, 1H), 2.56 (s, 1H), 2.59 (s, 6H). ^{13}C NMR (CDCl_3 , 100 MHz): δ (ppm) 144.66, 139.11, 133.27, 131.99, 128.59, 128.00, 126.15, 125.07, 121.33, 119.40, 15.66, 15.45. HRMS (APCI) m/z : $[\text{M}+\text{H}]^+$ Calcd for $\text{C}_{13}\text{H}_{11}\text{F}_3\text{O}_3\text{S}_3$: 368.9896, found 368.9886.

***(E)*-1,2-Bis(3,6-bis(methylthio)naphthalen-2-yl)ethene (11)**



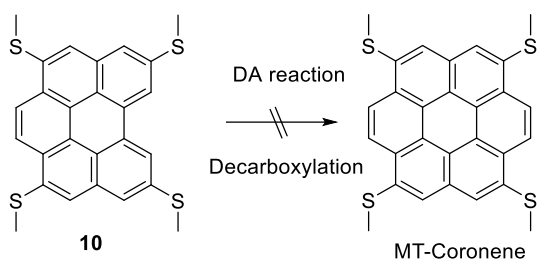
A solution of **10** (1.11 g, 3 mmol), *trans*-1,2-bis(tributylstannyl)ethene (0.79 mL 1.5 mmol), and tetrakis(triphenylphosphine)palladium(0) ($\text{Pd}(\text{PPh}_3)_4$, 173 mg, 0.156 mmol) in DMF (6 mL) was stirred at 100 °C in dark for 19 h. Then, the reaction mixture was dissolved in dichloromethane (150 mL), which was washed with water and brine and dried over MgSO_4 (anhydrous). After the solution was concentrated, the resulting residue was purified by silica gel column chromatography (containing 10 wt% K_2CO_3 , eluent: dichloromethane) and recrystallization from toluene to give **11** as a yellow solid (522 mg, 75%). Mp 211–214.9 °C. ^1H NMR (CDCl_3 , 400 MHz) δ (ppm) 8.01 (s, 1H), 7.74–7.72 (d, $J = 8.1$ Hz, 1H), 7.61 (s, 1H), 7.55 (s, 1H), 7.49 (s, 1H), 7.32–7.30 (dd, $J = 8.1, 1.8$ Hz, 1H), 2.60 (s, 6H). ^{13}C NMR (CDCl_3 , 100 MHz): δ (ppm) 137.09, 136.90, 134.22, 133.86, 129.29, 128.25, 128.11, 124.25, 125.02, 122.79, 121.73, 16.29, 15.71. HRMS (APCI) m/z : $[\text{M}+\text{H}]^+$ Calcd for $\text{C}_{26}\text{H}_{24}\text{S}_4$: 465.0834, found 465.0811.

***3,6,9,12*-Tetrakis(methylthio)benzo[ghi]perylene (12)¹¹**



A solution of **11** (278.8 mg, 0.6 mmol) and iodine (22.8 mg, 0.18 mmol) in toluene (360 mL) was irradiated with 27W black light for 13h under air. The solvent was evaporated, and the resulting solid was dissolved in chloroform (50 mL). The mixture was successively washed with aqueous sodium thiosulfate solution and dried over MgSO_4 , concentrated in vacuo. The crude product was further purified by silica gel column chromatography, eluted with dichloromethane. Recrystallization from toluene gave **12** as a yellow solid (196.5 mg, 70%). Mp 320–324 °C. ^1H NMR (CDCl_3 , 400 MHz) δ (ppm) 8.78 (s, 2H), 8.77 (s, 2H), 7.97 (s, 2H), 7.83 (s, 2H), 2.79 (s, 12H). ^{13}C NMR (CDCl_3 , 100 MHz): δ (ppm) peak was not found due to very low solubility. HRMS (MALDI-TOF) m/z : $[\text{M}]^+$ Calcd. for $\text{C}_{26}\text{H}_{20}\text{S}$: 460.0448, found 460.0464, Anal. Calcd for $\text{C}_{26}\text{H}_{20}\text{S}_4$: C, 67.79; H, 4.38%. Found: C, 67.61; H, 4.36%.

Attempted synthesis of MT-Coronene by Diels-Alder reaction followed by decarboxylation¹²



Under nitrogen atmosphere, **10** (100 mg, 0.22 mmol), *p*-chloranil (130 mg, 0.55 mmol) and maleic anhydride (1.2.0 g, 11 mmol) were heated 200 °C for 3 h. To the mixture, *p*-xylene (7 mL) was added and refluxed for 1 h. After cooling, the mixture was diluted with ether (10 mL), and the resulting precipitate was collected by filtration. The filtrate was treated with refluxing solvents (chloroform/ethyl acetate 1:2 v/v, 20 mL) to get the Diels-Alder adduct. The above product (120 mg, 0.22 mmol) was suspended in quinoline (20 mL), and Cu₂O (380 mg, 2.64 mmol) and Cu (40 mg, 0.55 mmol) were added to the suspension. The mixture was heated at 220 °C for 20 h, cooled to room temperature, and diluted with hydrochloric acid aqueous solution (10%, 100 mL). Sublimation under vacuum was tried, but no target compound was detected.

3. Theoretical calculations

The HOMO energy levels of MT-coronene, MO-coronene, **5** and **12**, together with the related parent PAHs, were calculated by using the Gaussian 16 program at B3lyp/6-31g(d,p) level.³

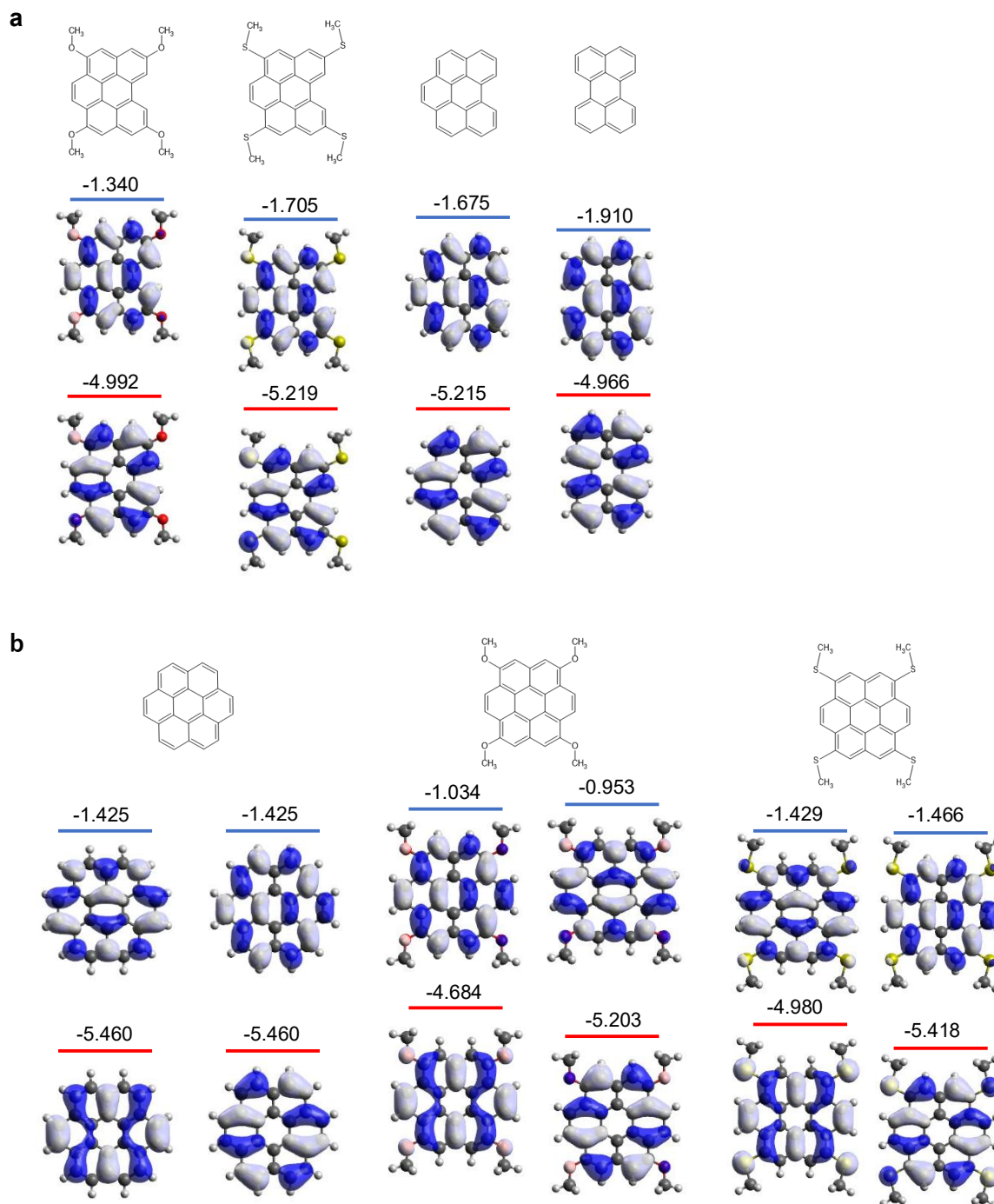


Fig. S2. Calculated HOMOs and LUMOs of MT-coronene, MO-coronene, **5** and **12**. (a) The methoxy groups of **5** push the HOMO energy level up to facilitate the reactivity in the Diels-Alder reaction as the enophile. On the other hand, the electron-donating effect of methylthio groups is lower than that of the methoxy groups, resulting in the relatively low-lying HOMO energy level. (b) Introduction of methylthio or methoxy groups on the coronene core breaks the degeneration of the HOMO and LUMO of parent coronene, resulting in similar HOMO distribution to those of MT-pyrene and MT-peropyrene.

4. Single-crystal X-ray analysis

For single-crystal X-ray structural analysis and single-crystal field-effect transistors, single crystals were grown by the physical vapor transport (PVT) and micro-spacing sublimation techniques under a nitrogen atmosphere. Single-crystal X-ray structural analyses were performed on a Rigaku Oxford Diffraction XtaLAB Synergy Custom DW apparatus with a HyPix-6000HE detector (CuK α radiation, $\lambda = 1.5418 \text{ \AA}$, and multilayer confocal optics). The crystal structures were solved and refined by the SHELXT¹⁴ and SHELXL¹⁵ programs, respectively. Non-hydrogen atoms underwent anisotropic refinement. All computational procedures were conducted using the crystallographic software Olex2 (version 1.5.0).¹⁶

Table S2. Crystallographic parameters of MT-coronene.

Temperature / K	300	200	100
Compound	MT-coronene	MT-coronene	MT-coronene
Formula	C ₂₈ H ₂₀ S ₄	C ₂₈ H ₂₀ S ₄	C ₂₈ H ₂₀ S ₄
Molecular Weight	484.01	484.01	484.01
Crystal Habit	plate	plate	plate
Crystal System	<i>triclinic</i>	<i>triclinic</i>	<i>triclinic</i>
Space Group	<i>P</i> -1	<i>P</i> -1	<i>P</i> -1
<i>a</i> / \AA	5.2372(2)	5.2396(2)	5.2197(3)
<i>b</i> / \AA	8.8932(3)	8.8512(2)	8.8113(3)
<i>c</i> / \AA	11.4399(4)	11.4251(3)	11.4168(6)
α / $^\circ$	88.844(3)	88.761(2)	88.594(3)
β / $^\circ$	77.845(3)	77.638(3)	77.550(5)
γ / $^\circ$	86.230(3)	86.513(3)	86.718(4)
<i>V</i> / \AA^3	519.74(3)	516.60(3)	511.86(4)
<i>Z</i>	1	1	1
<i>R</i>	0.0832	0.0469	0.0569
<i>R</i> _w	0.2268	0.1396	0.1668
GOF	1.130	1.070	1.044
CCDC	2446632	2446630	2446627

Table S3. Crystallographic parameters of MO-coronene.

Temperature / K	300	200	100
Compound	MO-coronene	MO-coronene	MO-coronene
Formula	C ₂₈ H ₂₀ O ₄	C ₂₈ H ₂₀ O ₄	C ₂₈ H ₂₀ O ₄
Molecular Weight	420.46	420.46	420.46
Crystal Habit	block	block	block
Crystal System	<i>monoclinic</i>	<i>monoclinic</i>	<i>monoclinic</i>
Space Group	<i>P2₁/n</i>	<i>P2₁/n</i>	<i>P2₁/n</i>
<i>a</i> / Å	10.9191(4)	10.8892(4)	10.8606(3)
<i>b</i> / Å	13.1598(6)	13.0557(4)	12.9849(4)
<i>c</i> / Å	13.7566(5)	13.7463(5)	13.7224(4)
α / °	90	90	90
β / °	102.816(3)	102.879(4)	103.074(3)
γ / °	90	90	90
<i>V</i> / Å ³	1927.47(13)	1905.09(12)	1885.02(10)
<i>Z</i>	4	4	4
<i>R</i>	0.0602	0.0575	0.0606
<i>R_w</i>	0.1585	0.1534	0.1535
GOF	1.035	1.030	1.079
CCDC	2446629	2446628	2446631

Table S4. Crystallographic parameters of **5**.

Temperature / K	300	200	100
Compound	5	5	5
Formula	C ₂₆ H ₂₀ O ₄	C ₂₆ H ₂₀ O ₄	C ₂₆ H ₂₀ O ₄
Molecular Weight	396.44	396.44	396.44
Crystal Habit	plate	plate	plate
Crystal System	<i>monoclinic</i>	<i>monoclinic</i>	<i>monoclinic</i>
Space Group	<i>P2₁/n</i>	<i>P2₁/n</i>	<i>P2₁/n</i>
<i>a</i> / Å	9.7680(4)	9.7178(7)	9.6782(4)
<i>b</i> / Å	10.9262(3)	10.8952(6)	10.8375(4)
<i>c</i> / Å	17.4458(5)	17.3430(10)	17.2665(6)
α / °	90	90	90
β / °	91.678(3)	91.835(6)	92.011(3)
γ / °	90	90	90
<i>V</i> / Å ³	1861.14(11)	1835.3(2)	1809.92(12)
<i>Z</i>	4	4	4
<i>R</i>	0.0888	0.0819	0.0993
<i>R_w</i>	0.2028	0.2384	0.2171
GOF	1.162	1.103	1.208
CCDC	2446635	2446634	2446633

Table S5. Crystallographic parameters of **5** (minor polymorph).

Temperature / K	300	200	100
Compound	5	5	5
Formula	C ₂₆ H ₂₀ O ₄	C ₂₆ H ₂₀ O ₄	C ₂₆ H ₂₀ O ₄
Molecular Weight	396.44	396.44	396.44
Crystal Habit	prism	prism	prism
Crystal System	<i>triclinic</i>	<i>triclinic</i>	<i>triclinic</i>
Space Group	<i>P</i> -1	<i>P</i> -1	<i>P</i> -1
<i>a</i> / Å	10.9983(3)	10.9472(2)	10.8935(2)
<i>b</i> / Å	18.9426(4)	18.8237(3)	18.7430(4)
<i>c</i> / Å	19.1861(3)	19.0718(2)	18.9847(3)
α / °	86.1432(16)	85.8795(11)	85.8831(14)
β / °	75.6762(19)	75.9202(14)	76.1584(16)
γ / °	79.232(2)	79.8080(14)	79.9947(18)
<i>V</i> / Å ³	3803.79(16)	3750.11(11)	3704.58(13)
<i>Z</i>	8	8	8
<i>R</i>	0.0533	0.0503	0.0482
<i>R</i> _w	0.1630	0.1540	0.1406
GOF	1.025	1.026	1.044
CCDC	2446637	2446636	2446638

Table S6. Crystallographic parameters of **12**.

Temperature / K	300	200	100
Compound	12	12	12
Formula	C ₂₆ H ₂₀ S ₄	C ₂₆ H ₂₀ S ₄	C ₂₆ H ₂₀ S ₄
Molecular Weight	460.69	460.69	460.69
Crystal Habit	prism	prism	prism
Crystal System	<i>triclinic</i>	<i>triclinic</i>	<i>triclinic</i>
Space Group	<i>P</i> -1	<i>P</i> -1	<i>P</i> -1
<i>a</i> / Å	5.10100(10)	5.09140(10)	5.0737(2)
<i>b</i> / Å	9.13620(10)	9.07180(10)	9.0307(2)
<i>c</i> / Å	11.3735(2)	11.3386(2)	11.3090(5)
α / °	89.639(2)	89.4690(10)	89.351(3)
β / °	77.413(2)	77.308(2)	77.263(3)
γ / °	87.3650(10)	87.6390(10)	87.865(2)
<i>V</i> / Å ³	516.758(15)	510.479(15)	505.06(3)
<i>Z</i>	1	1	1
<i>R</i>	0.0752	0.0808	0.0771
<i>R</i> _w	0.2086	0.2241	0.1814
GOF	1.114	1.228	1.182
CCDC	2446641	2446640	2446639

5. Photoemission yield spectroscopy

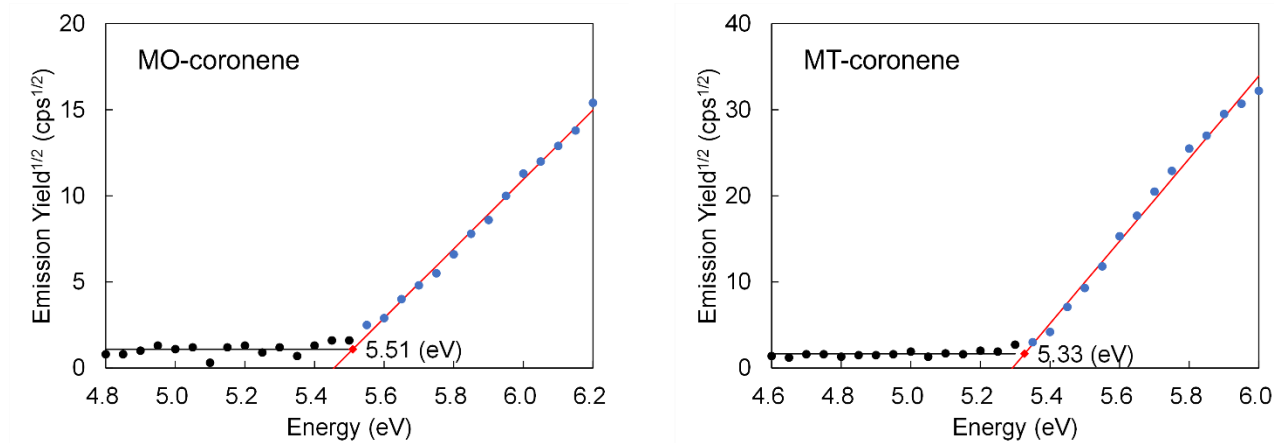


Fig. S3. Ionization energies of MO-coronene (left) and MT-coronene (right) single crystals measured on a RIKEN-Keiki AC-2 system in air.

6. Out-of-plane XRD

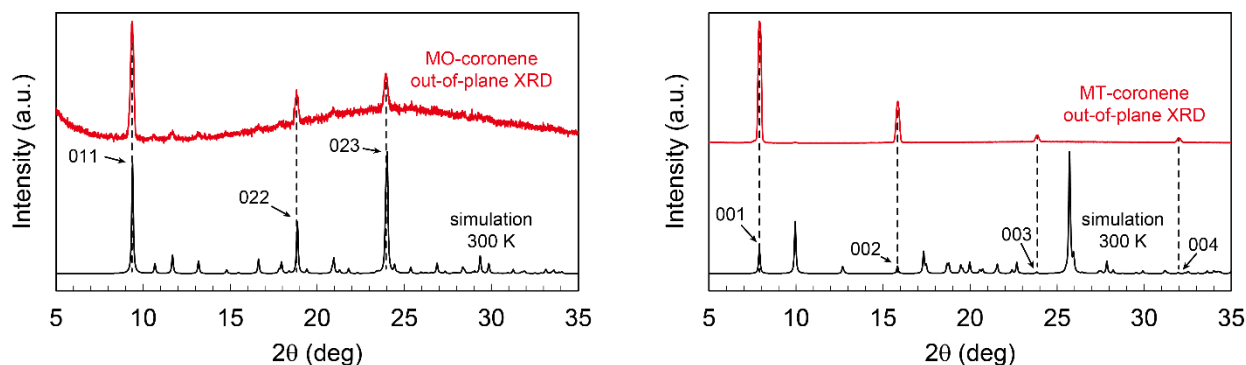


Fig. S4. Out-of-plane XRD of MO-coronene (left) and MT-coronene (right) single crystals grown by micro-spacing sublimation.

7. Crystal structures of **5** and **12**

5 gave two polymorphs, both of which were classified into the sandwich herringbone structure similar to that of MO-coronene and parent benzo[*ghi*]perylene.¹⁷ The major polymorph consists of one crystallographically independent molecule with a disorder at the bay position and the corresponding benzene part of the benzo[*ghi*]perylene core: the occupancy of two carbon atoms at the benzene parts is *ca.* 50%, indicating the positional disorder of the molecule in the crystal, and as a result, the molecular structure itself looks like MO-coronene. Like the crystal structure of MO-coronene, the packing structure of **5** is a sandwich herringbone structure with $P2_1/n$ space group ($Z = 4$), though they are not crystallographically isostructural. In the crystal structure of **5**, similar to that of MO-coronene, the methyl hydrogen atoms, together with the core hydrogen atoms, are involved in the CH- π intermolecular interaction (Fig. S3), and thus, it can be concluded that the role of the methoxy groups in MO-coronene and **5** is significantly different from those of methylthio groups of MT-coronene and other methylthiolated PAHs.¹⁸ The minor polymorph of **5** has a similar

sandwich herringbone structure to the major polymorph but with a different space group ($P-1$, $Z = 8$), in which the tetrameric structure of **5** without disorder is characteristic (Fig. S3).

The crystal structure of **12** was almost identical to that of MT-coronene (Fig. S3c, S3d) with slightly reduced volume (from 519.74 to 516.76 Å³). The shape of the molecule of **12**, determined by single-crystal X-ray analysis, also looked like MT-coronene due to disorder. Similarly to the disorder observed in one of the polymorphs of **5**, the occupancy of the carbons at the bay positions was *ca.* 50 %.

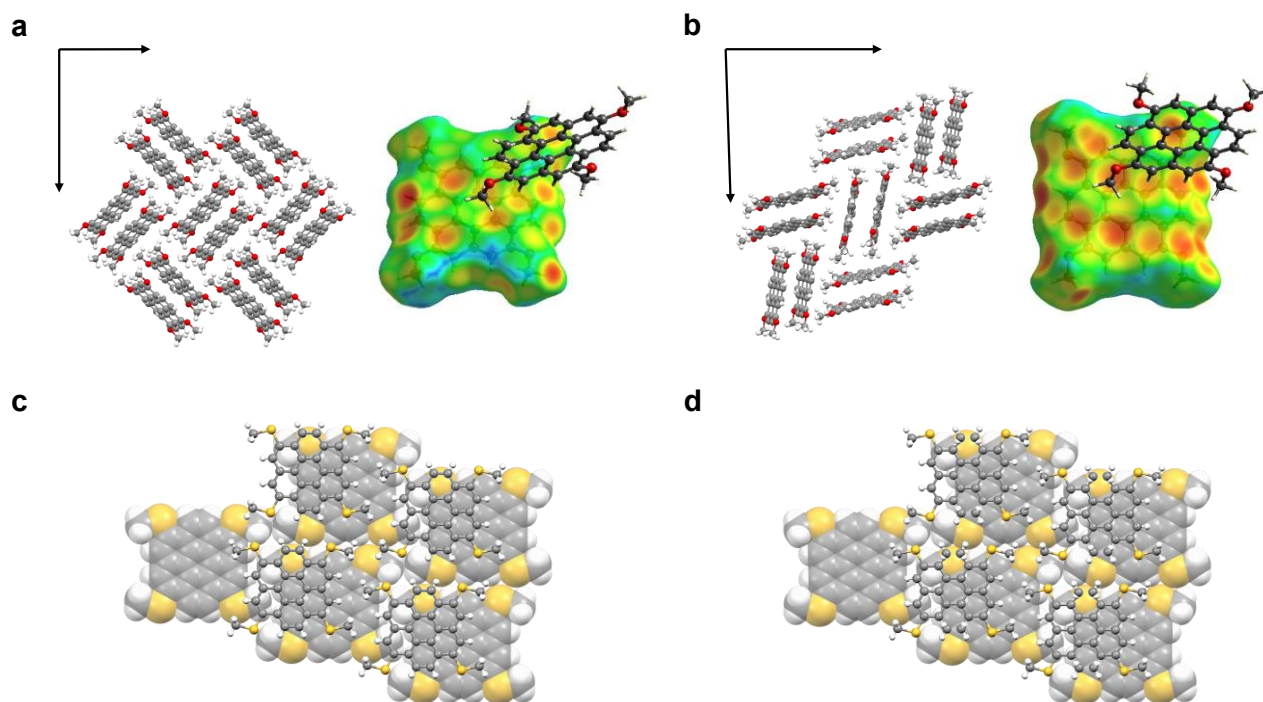


Fig. S5. Crystal structures of (a) **5**, $P2_1/n$ (b) **5**, $P-1$ together with the Hirshfeld surface mapped with d_e (distance external to the surface). Crystal structures of (c) MT-coronene and (d) **12**. Note that the molecular structure of **12** (d) looks identical to that of MT-coronene (c) due to disorder.

8. Crystal structures of methylthiolated naphthalene and perylene

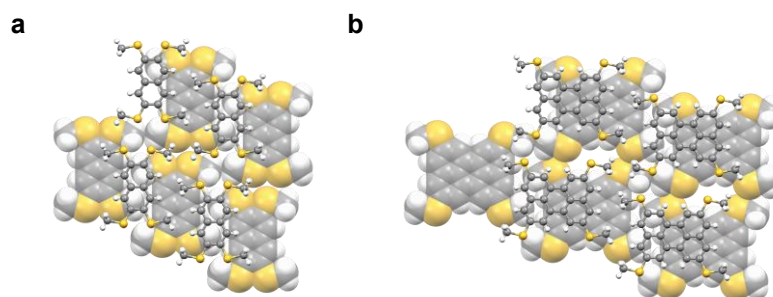


Fig. S6. Crystal structures of (a) methylthiolated naphthalene¹⁹ and (b) perylene⁷. Note that the spacing between two methylthiogroups is efficiently filled by the methylthio groups of adjacent molecules.

9. Single-crystal field-effect transistors (SC-FETs)

The crystals used for evaluating SC-FETs were grown using the physical vapor transport method. The free-standing plates obtained by growing them on glass substrates were transferred onto CYTOP-coated SiO₂/Si substrates using a tungsten needle. The SC-FETs of MT-coronene were completed by painting water-based colloidal graphite (EM-Science) on the sides of the crystals. The OFET operation was measured in air using a semiconductor parameter analyzer (Keithley SCS-4200). The temperature dependence of mobility was measured using a vacuum probe system (<10⁻³ Pa) with a cryostat (ExPP) at 5-minute intervals while cooling at a rate of 2.0 °C min⁻¹.

MO-coronene crystals were generally block-shaped and unsuitable for lamination in FET fabrication, but the smaller crystals were of an acceptable thickness. The size of such crystals (<20 μm) did not allow for graphite electrode formation by hand, and instead, the MoOx (15 nm)/Au (30 nm) electrodes were formed using a φ10 μm Au wire as a shadow mask. Fig. S5 shows the operation of the SC-FET of MO-coronene measured in air.

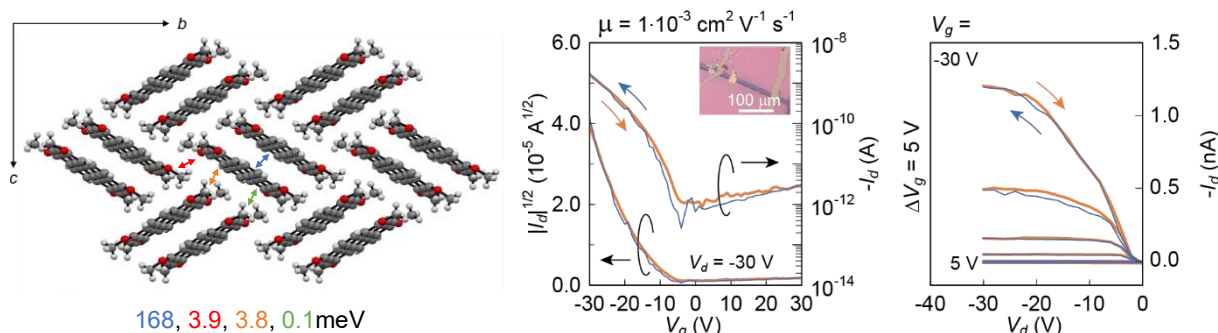


Fig. S7. Evaluation of MO-coronene as a semiconducting material. (a) Calculated ts based on the crystal structure. (b) transfer and (c) output characteristics of MO-coronene-based SC-FET measured in air.

10. Intermolecular overlap area

To examine how two-dimensional molecular displacement affects both orbital interactions and geometric overlap, we calculated the xy -projection overlap areas of π -stacked dimers at systematically varied lateral positions. For consistency with the transfer integral calculations described in the main text, the overlap areas were calculated for the same displacements as in Fig. 5; for each molecule in the series, one molecule was fixed at the origin, and a second identical copy was placed at $(x, y, z) = (0.4 \times n, 0.4 \times m, 3.5)$ Å, where n and m are integers. The overlap area was defined as the intersection area of the atomic van der Waals projections of the two molecules onto the xy -plane (Fig. S8, top). The atoms were modeled as two-dimensional disks with radii corresponding to their van der Waals values, and the overlap area was estimated using Monte Carlo integration with low-discrepancy Halton sampling (500,000 samples).²⁰ For each displacement, the corresponding transfer integral value was plotted against the calculated overlap area for the methylchalcogeno PAH series (Fig. S8, bottom).

Note that for most of the range of overlap areas, there exist multiple different overlap configurations corresponding to multiple possible transfer integral values. The transfer integrals in the experimental structure of MT-coronene are not among the highest possible values out of similar overlap areas. A similar tendency is observed for the other relatively low mobility material, MT-perylene although the distribution pattern is different from other PAHs because of the different shape of HOMO of MT-perylene (see Fig. 5 in the main text). On the other hand, high mobility materials such as MT-pyrene and MT-peropyrene have relatively large transfer integrals in two π -stacking directions, while moderate mobility MS-pyrene has a relatively large transfer integral only in one π -stacking direction. In most cases, much better orbital overlaps can be achieved in principle if the π -stacking configuration can be adjusted to the “hot spots” even without changing the overlap areas.

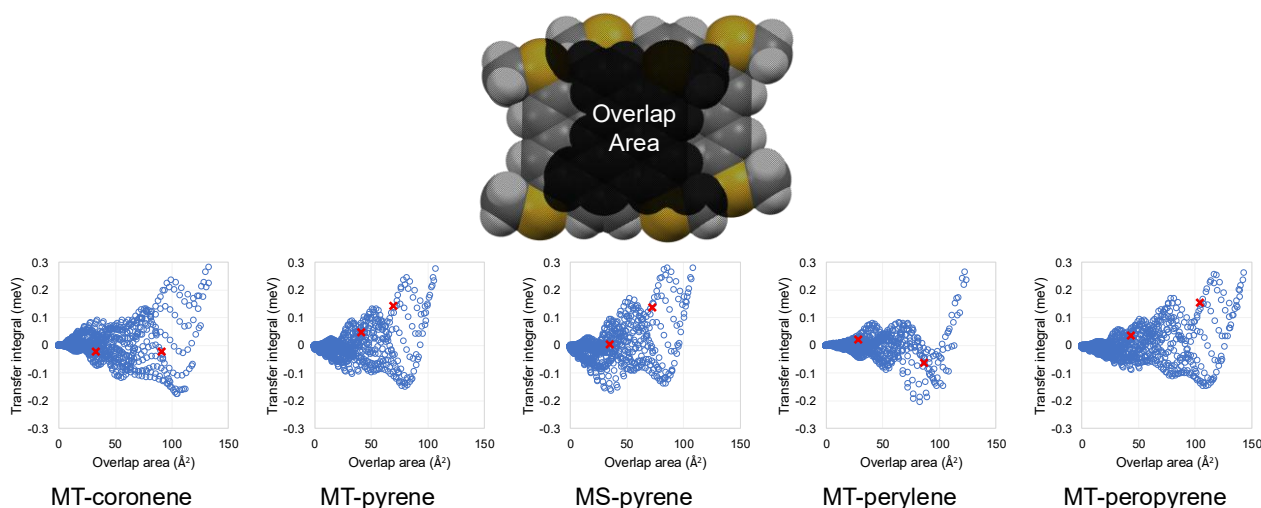


Fig. S8. Transfer integrals of the artificial π -stacking configurations with displacements $(x_1, y_1, z_1) = (0.4 \times n, 0.4 \times m, 3.5)$ Å (see Fig. 5) plotted against the corresponding intermolecular overlap area for MT-coronene, MT-pyrene, MS-pyrene, MT-perylene, and MT-peropyrene. The red crosses represent the values for experimental crystal structures.

11. NMR spectra

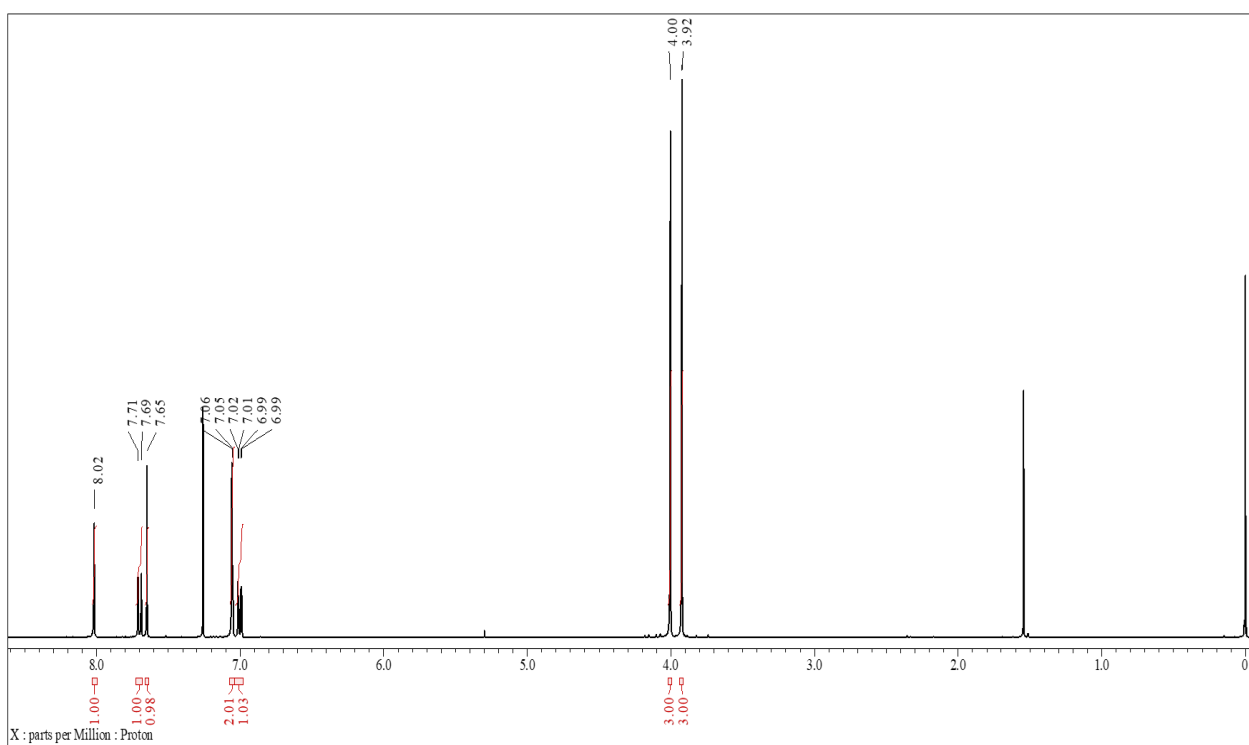


Fig. S9. ¹H NMR of **4** in CDCl₃.

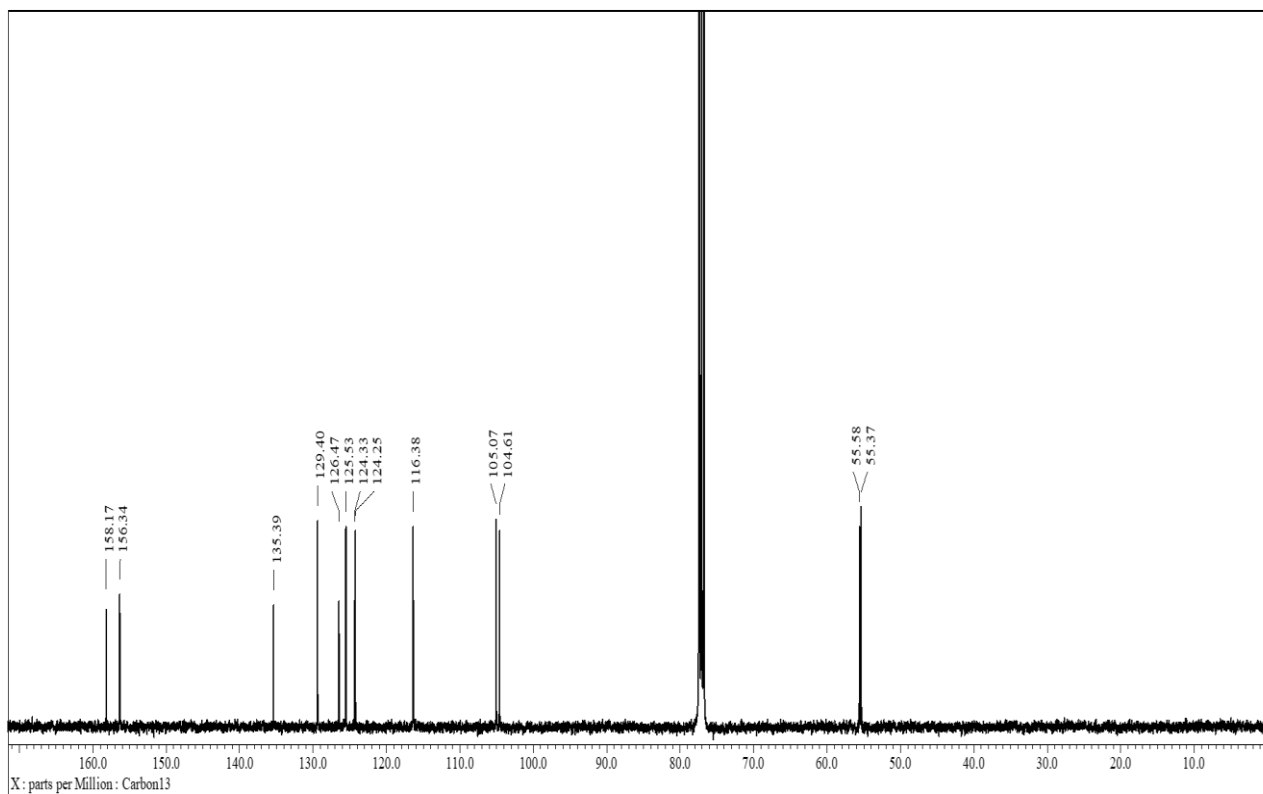


Fig. S10. ¹³C NMR of **4** in CDCl₃.

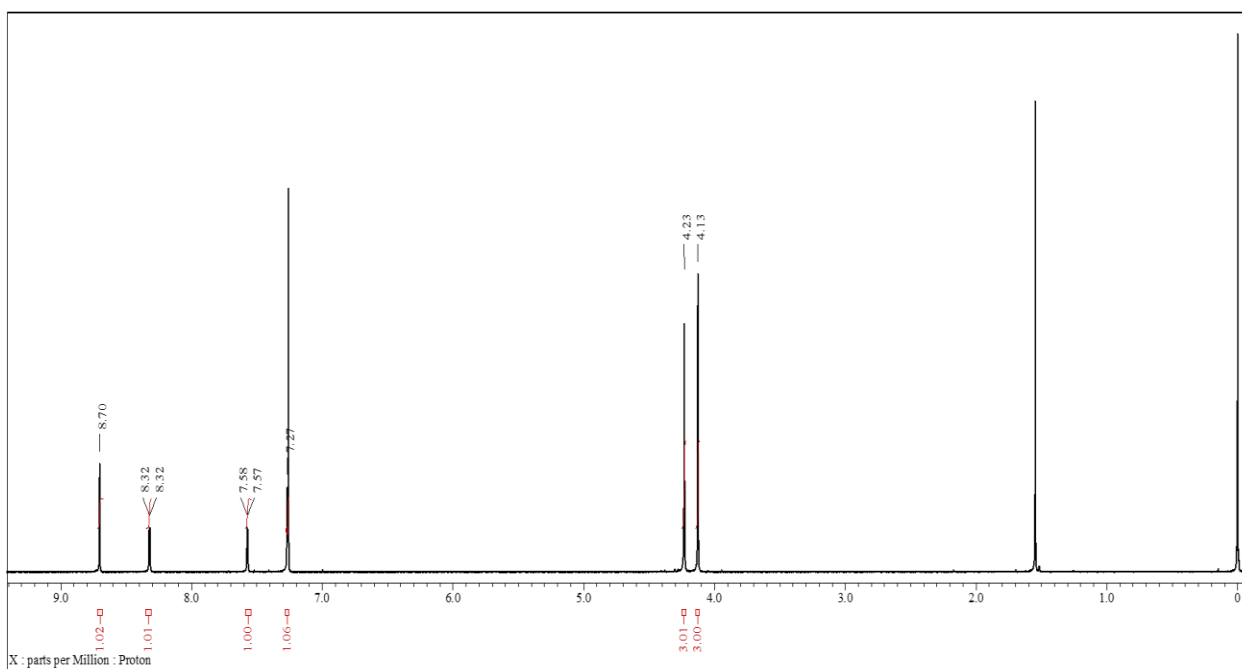


Fig. S11. ^1H NMR of **5** in CDCl_3 .

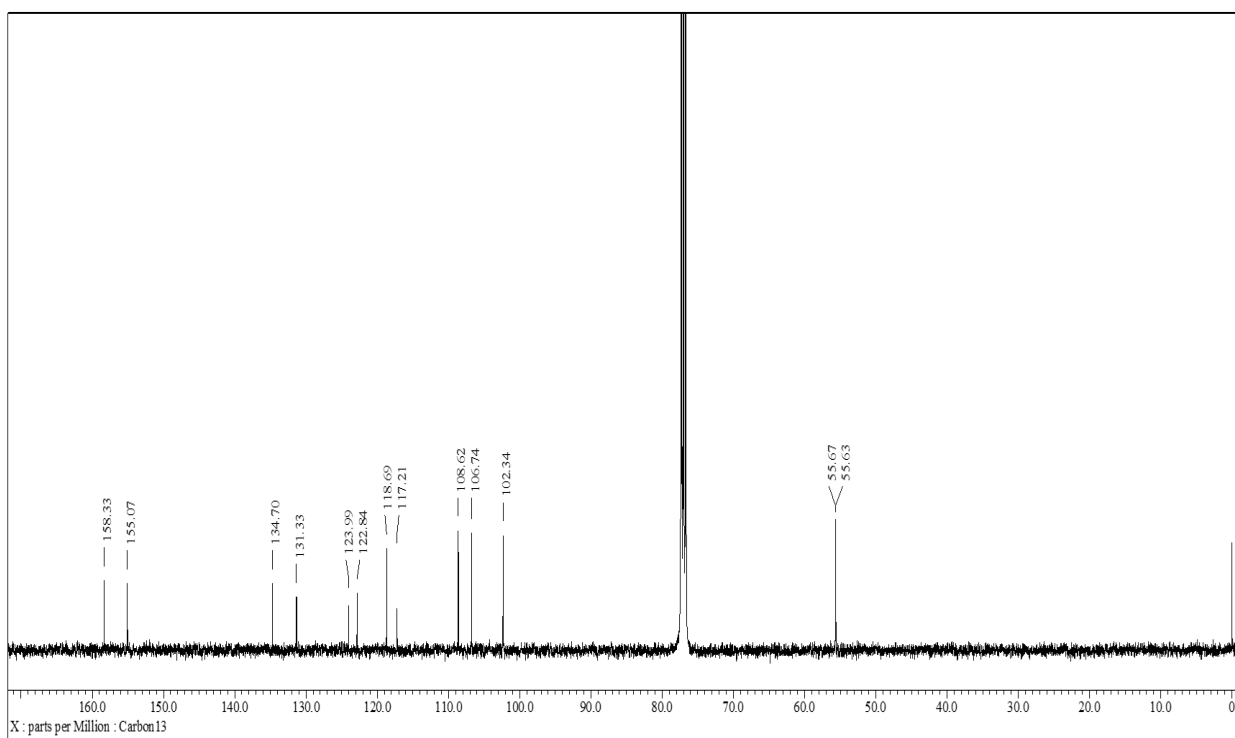


Fig. S12. ^{13}C NMR of **5** in CDCl_3 .

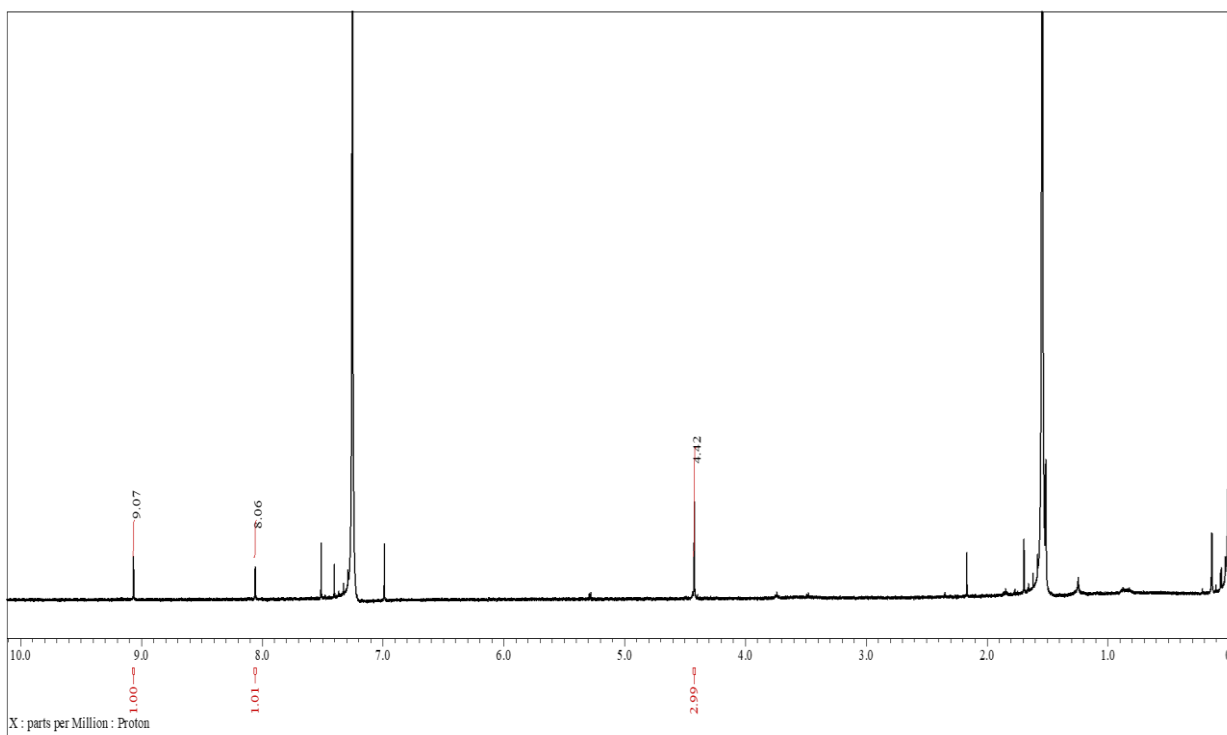


Fig. S13. ¹H NMR of MO-coronene in CDCl₃.

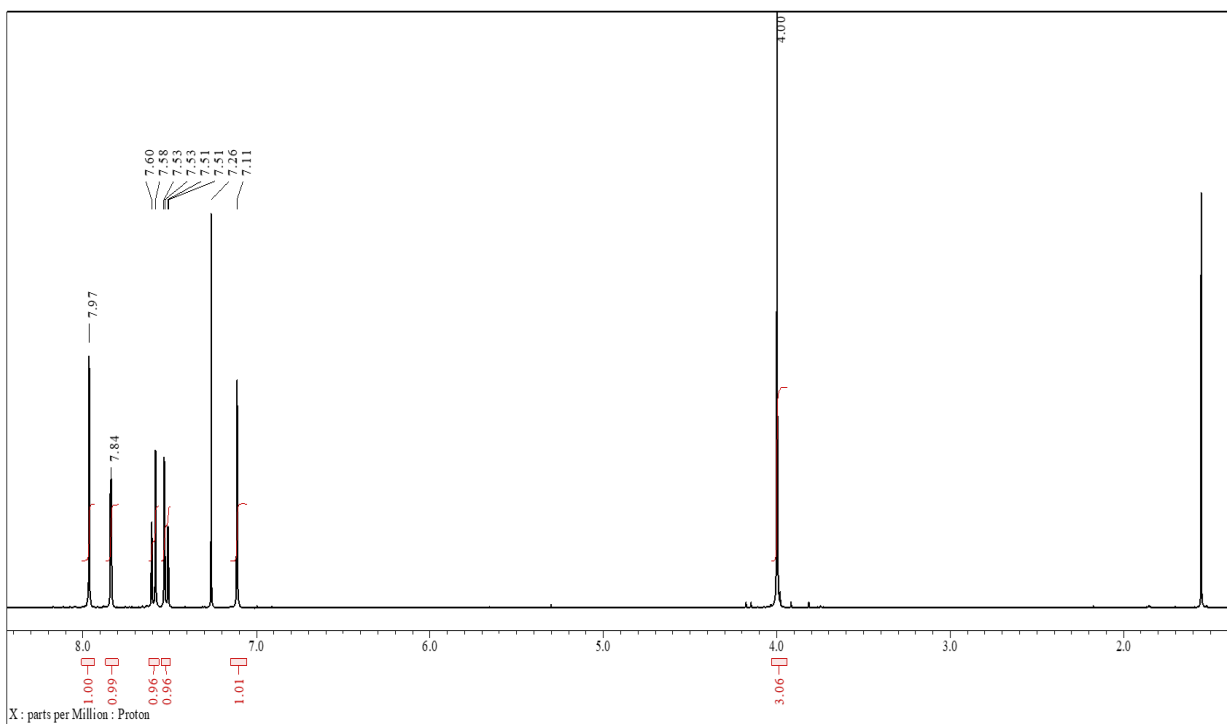


Fig. S14. ¹H NMR of 7 in CDCl₃.

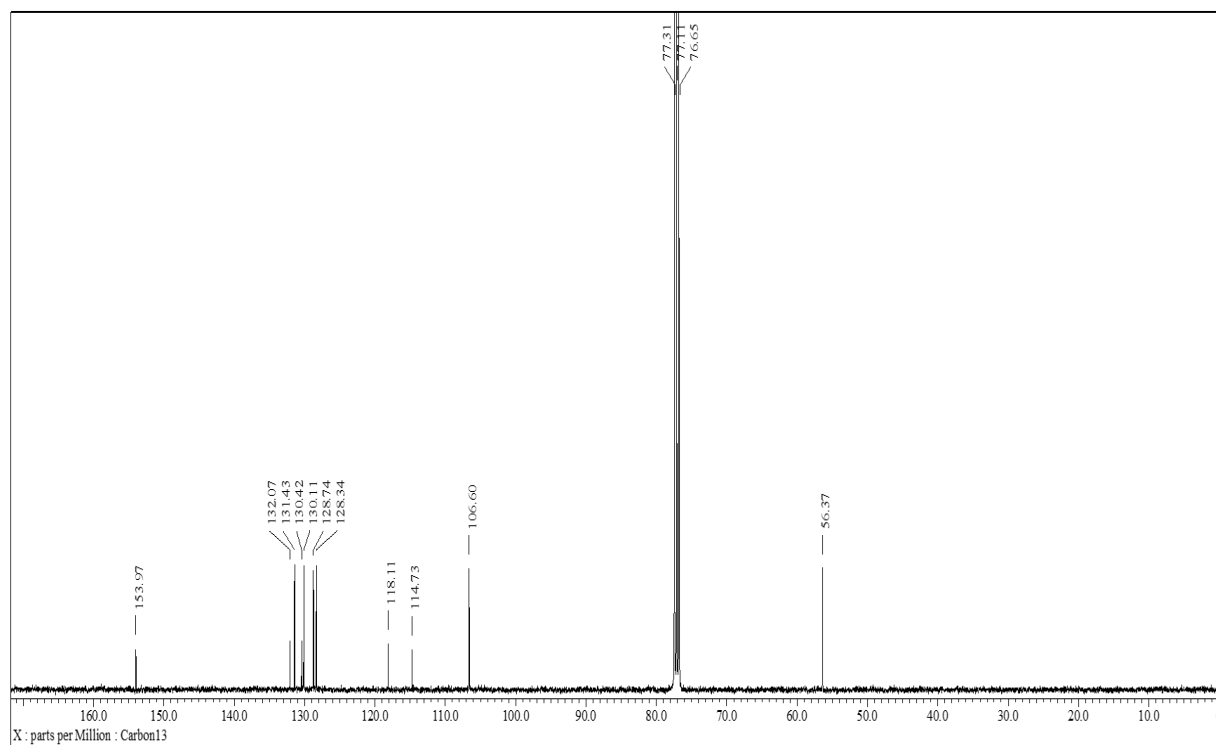


Fig. S15. ^{13}C NMR of **7** in CDCl_3 .

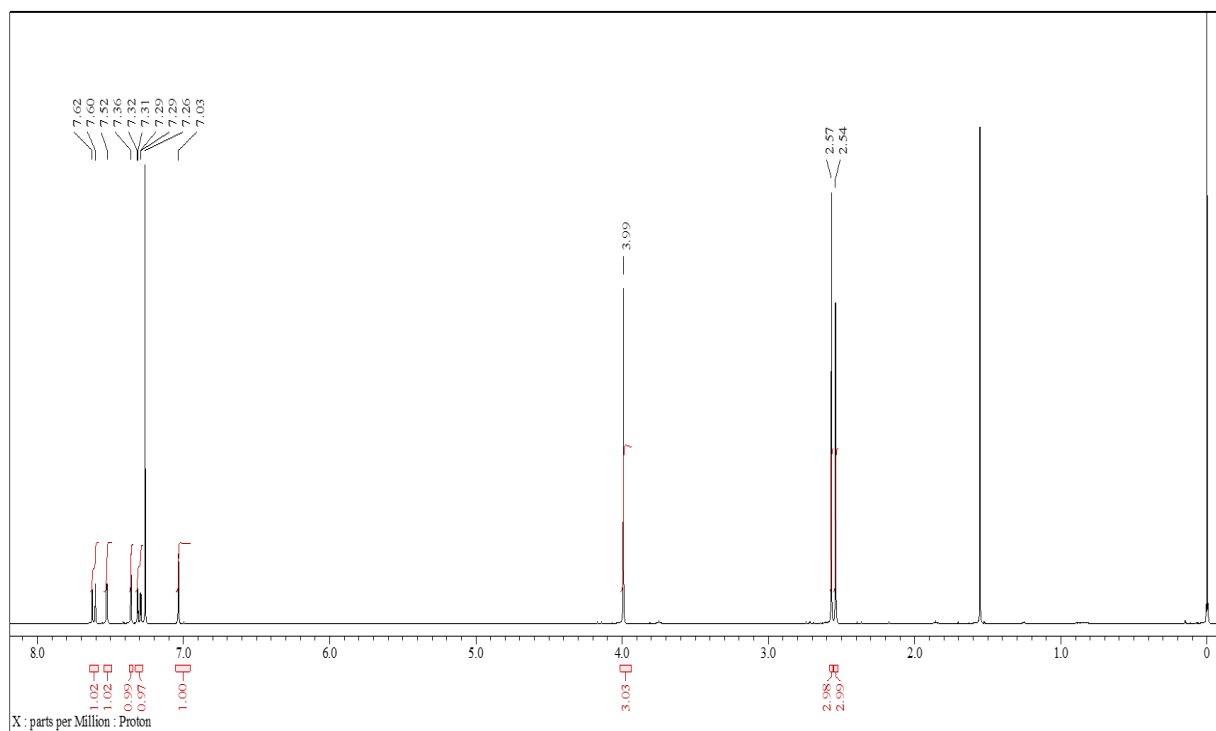


Fig. S16. ^1H NMR of **8** in CDCl_3 .

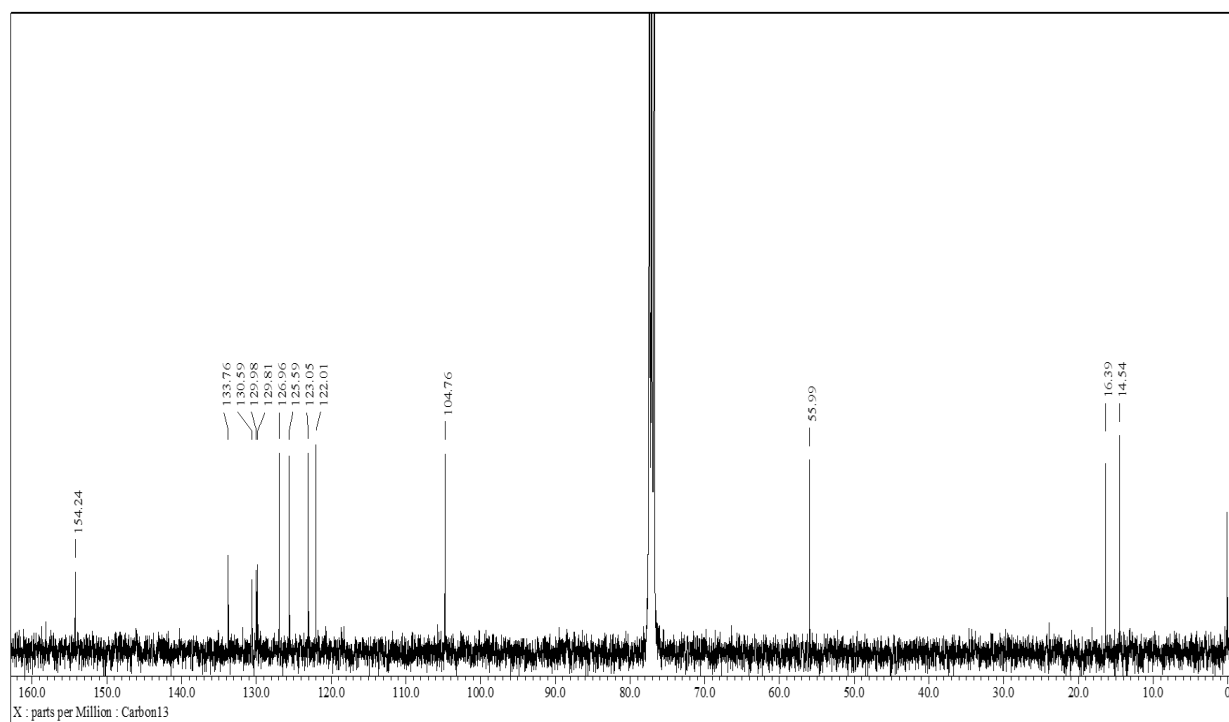


Fig. S17. ^{13}C NMR of **8** in CDCl_3 .

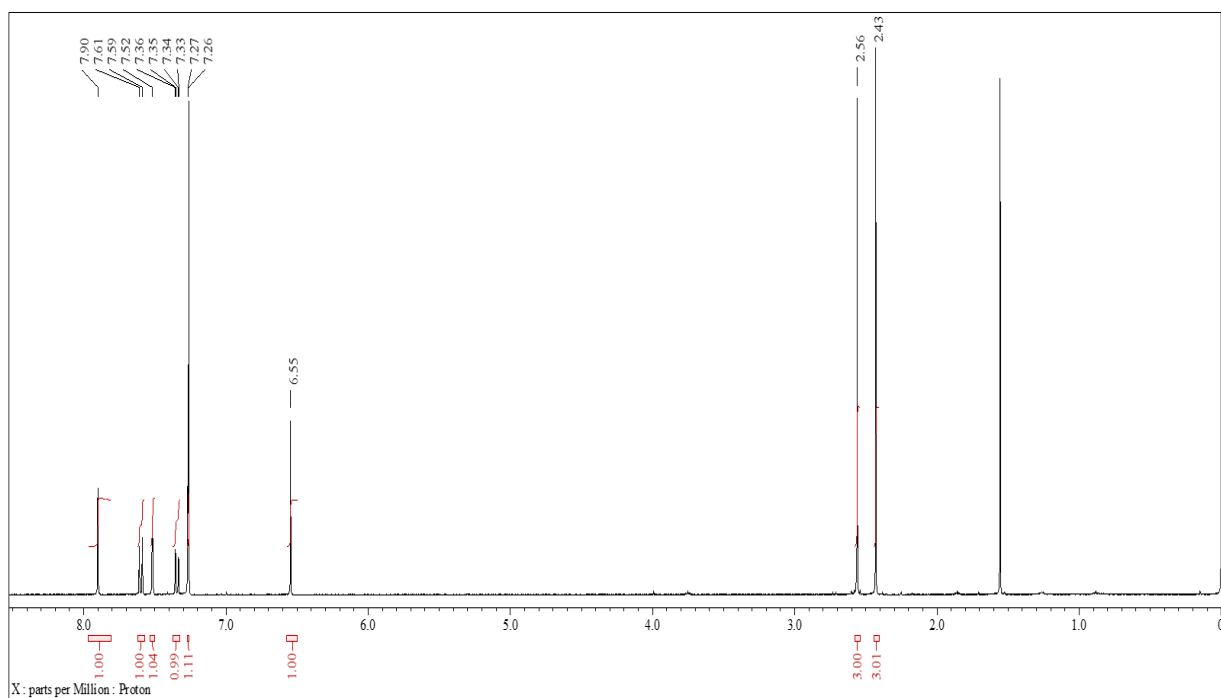


Fig. S18. ^1H NMR of **9** in CDCl_3 .

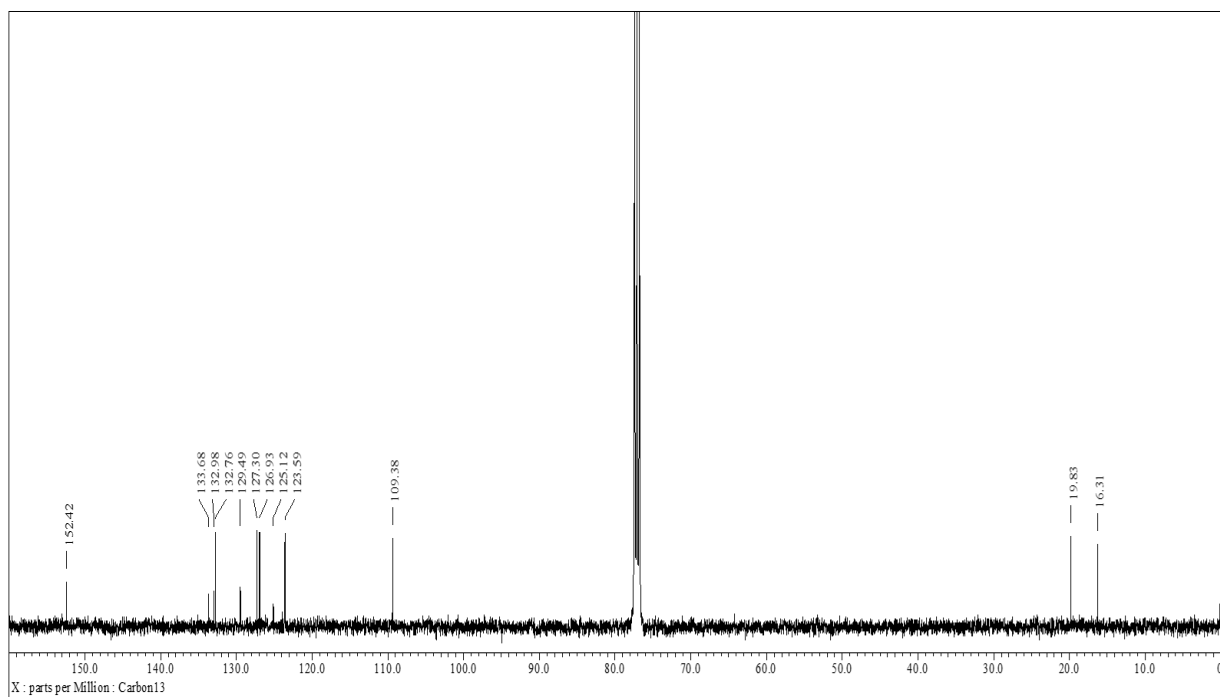


Fig. S19. ¹³C NMR of **9** in CDCl₃.

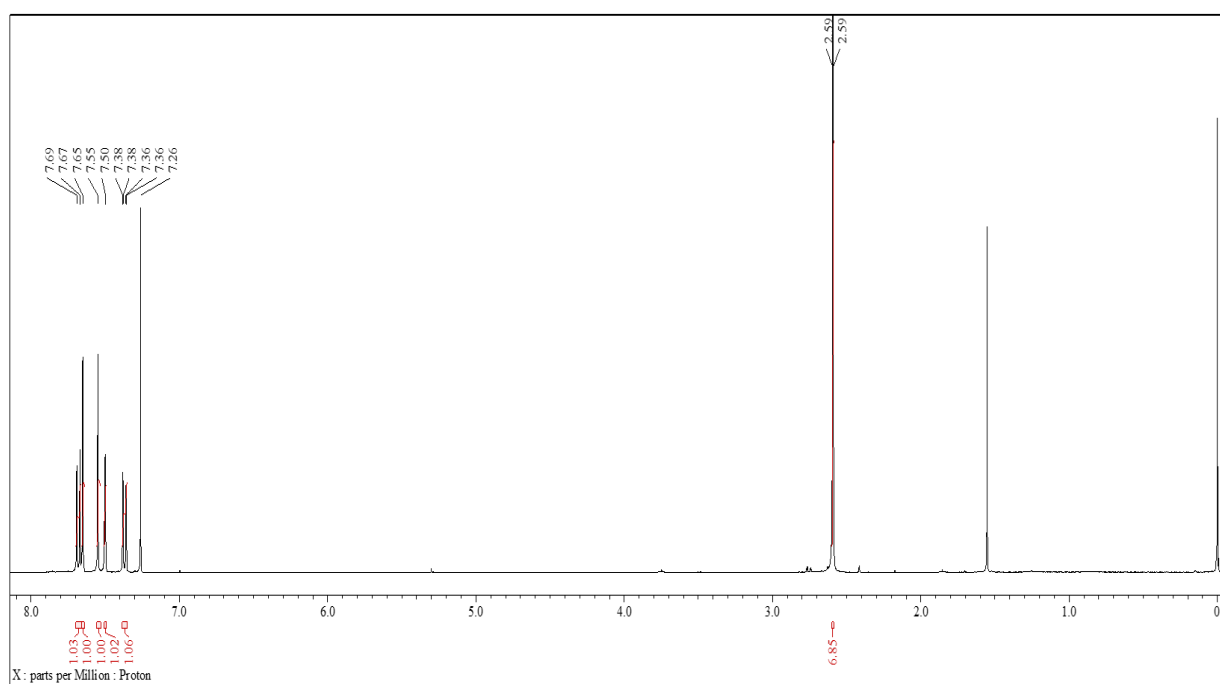


Fig. S20. ¹H NMR of **10** in CDCl₃.

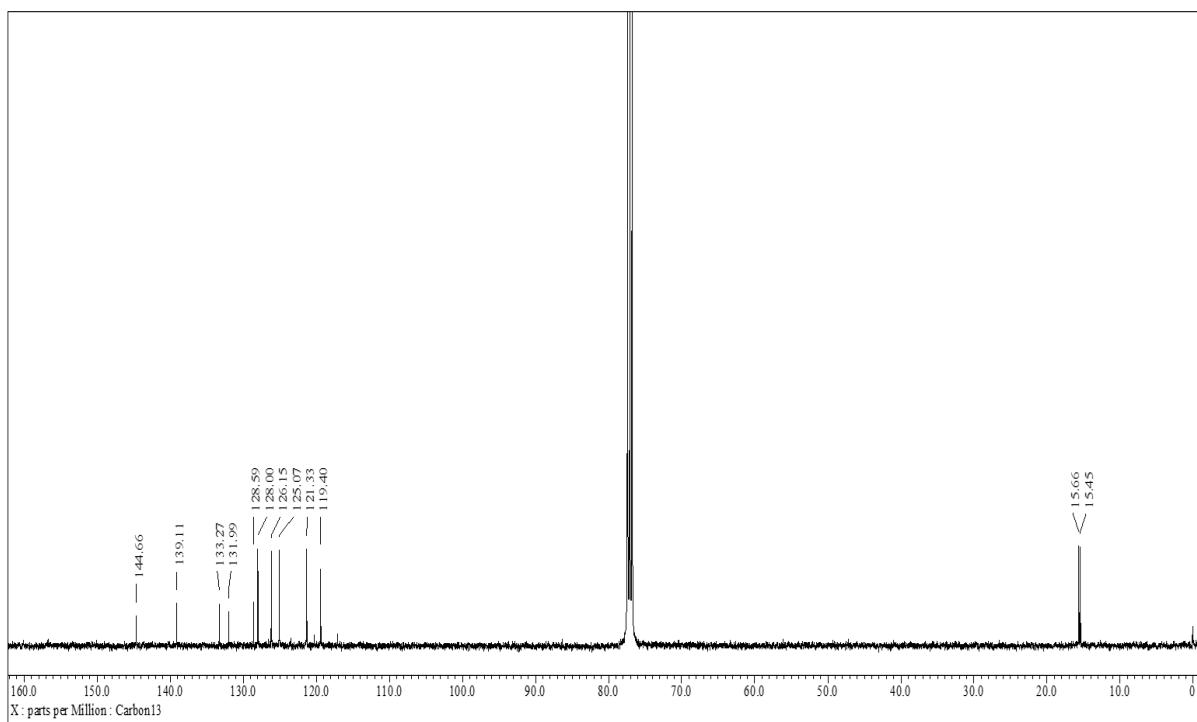


Fig. S21. ¹³C NMR of **10** in CDCl₃.

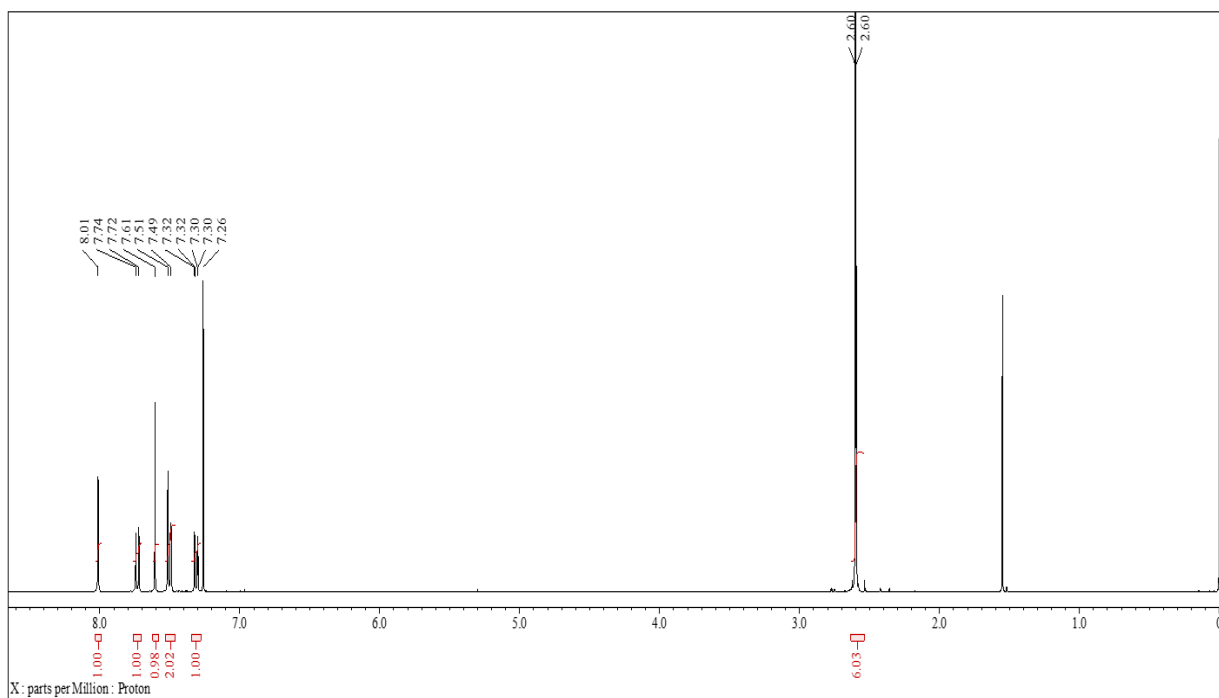


Fig. S22. ¹H NMR of **11** in CDCl₃.

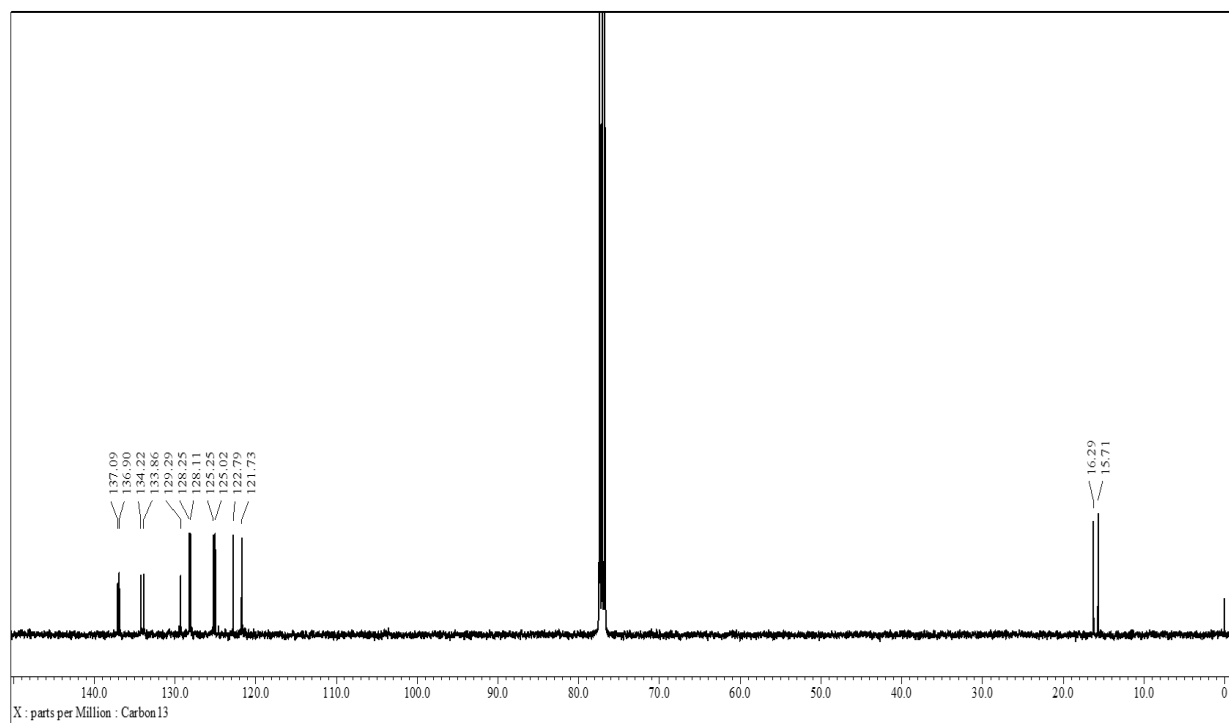


Fig. S23. ^{13}C NMR of **1** in CDCl_3 .

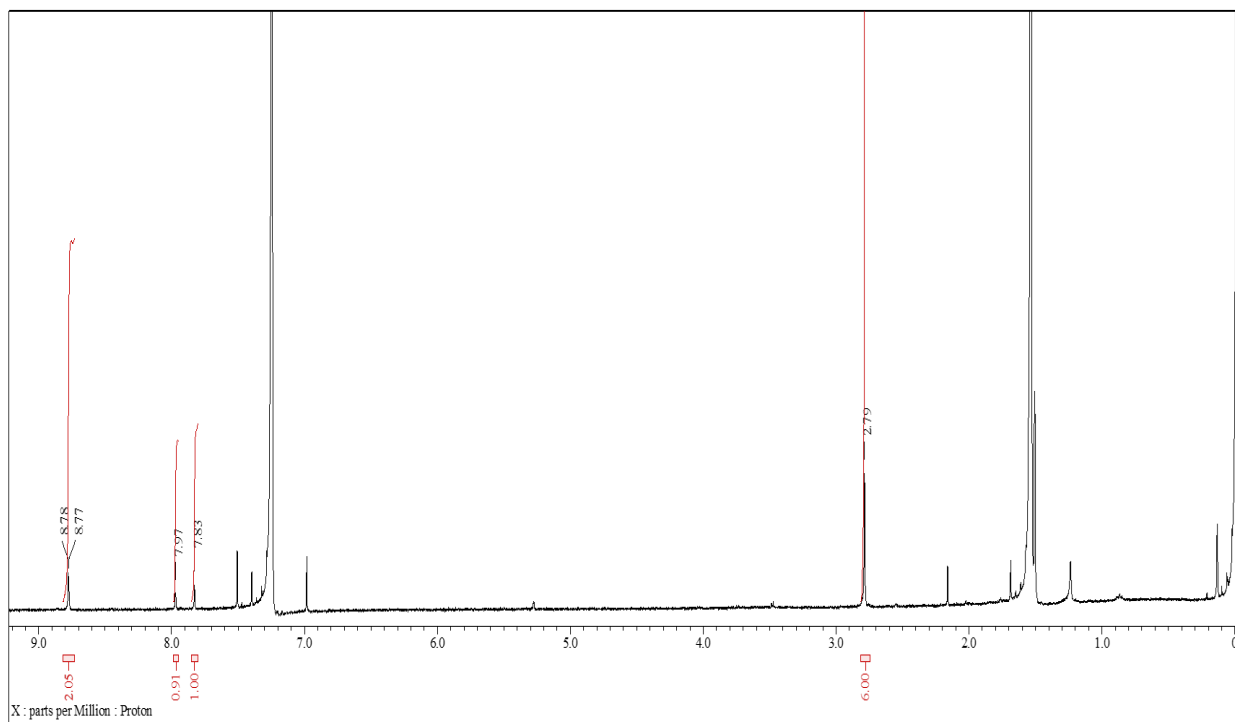


Fig. S24. ^1H NMR of **12** in CDCl_3 .

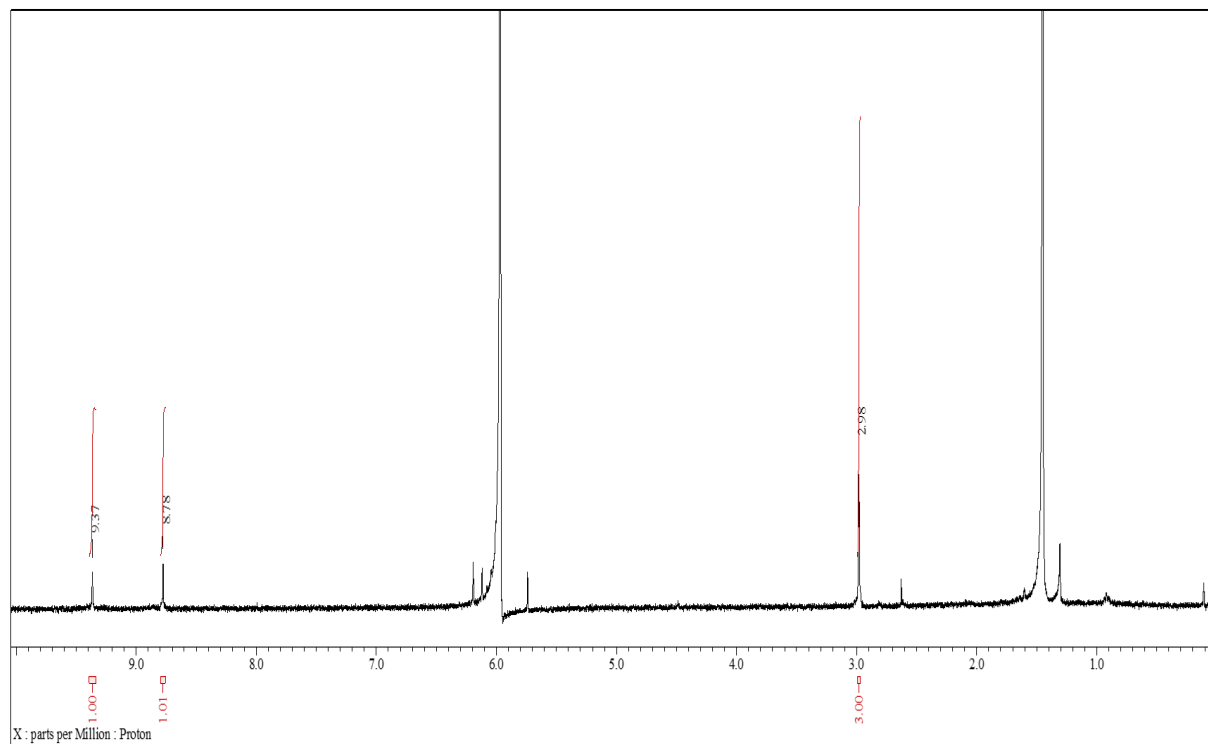


Fig. S25. ^1H NMR of MT-coronene in $1,1,2,2$ -tetrachloroethane- d_2 (TCE- d_2) at $100\text{ }^\circ\text{C}$ with high scan.

12. High-resolution MS spectra

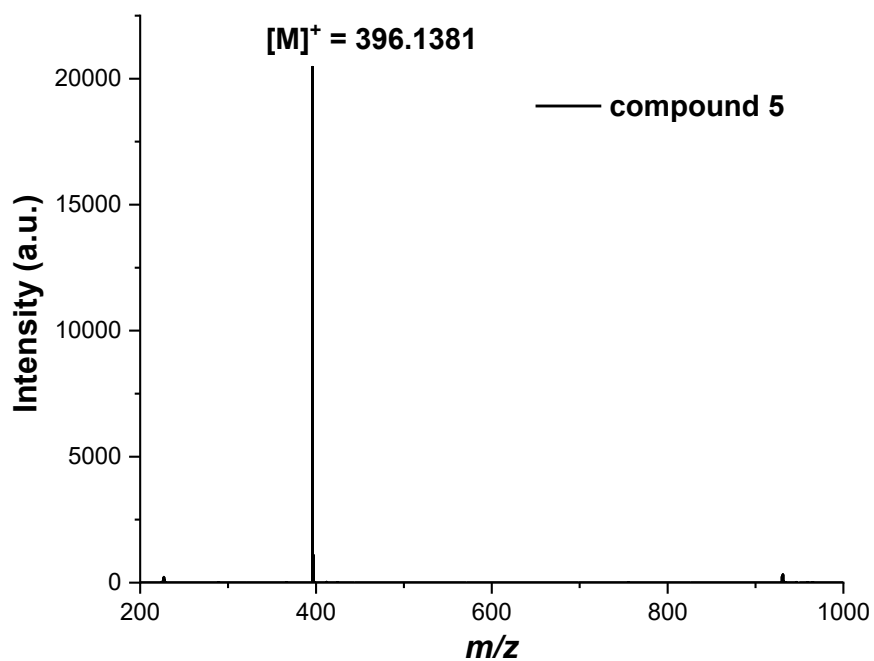


Fig. S26. HRMS (MALDI-TOF, in dithranol matrix) of **5**.

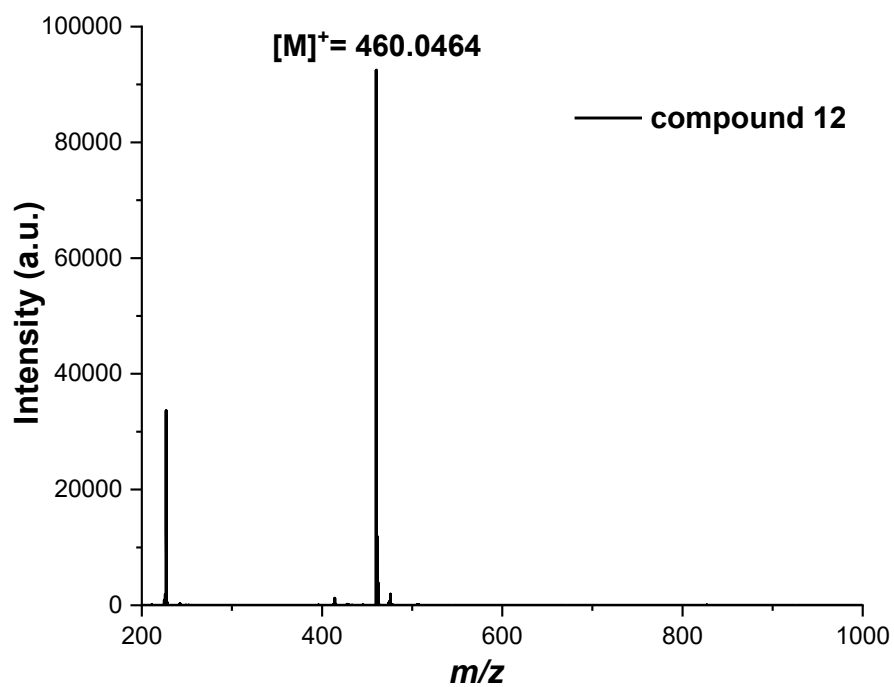


Fig. S27. HRMS (MALDI-TOF, in dithranol matrix) of **12**.

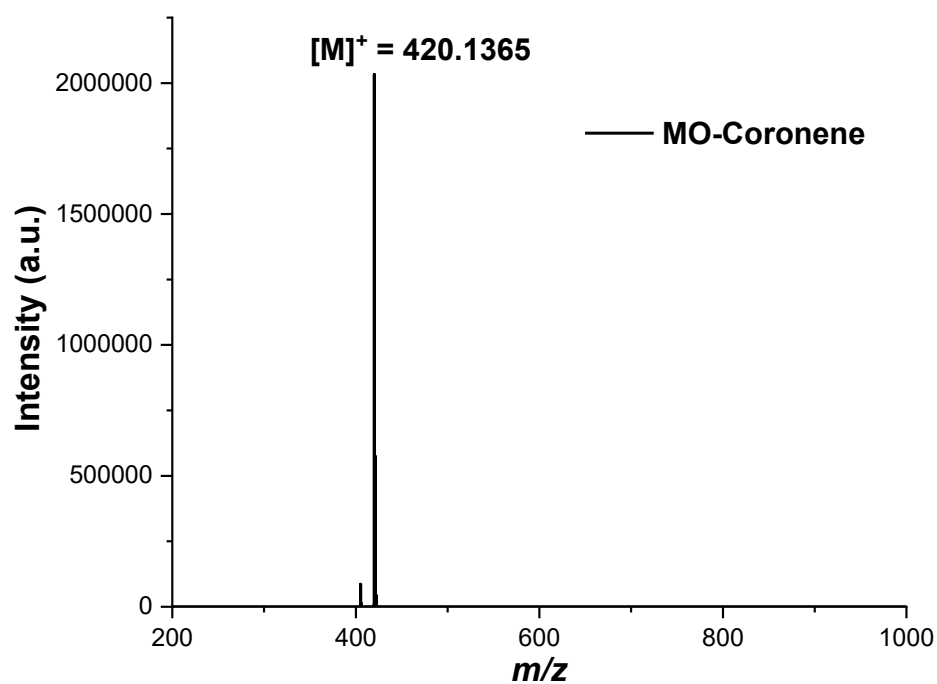


Fig. S28. HRMS (MALDI-TOF, in dithranol matrix) of MO-coronene.

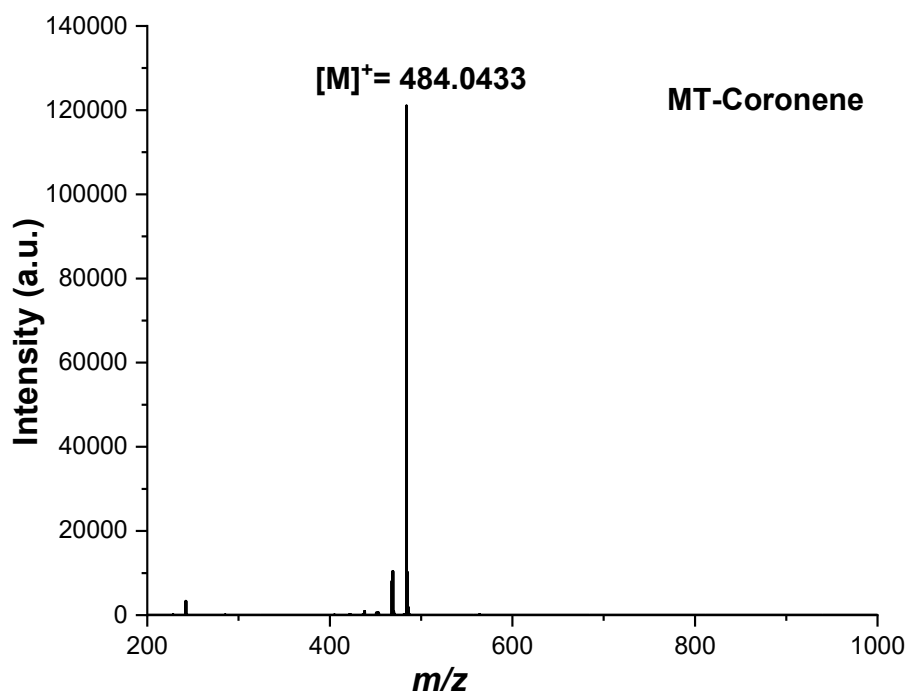


Fig. S29. HRMS (MALDI-TOF, in dithranol matrix) of MT-coronene.

13. APCI-MS and ¹H NMR spectra of crude MT-coronene

Spectrum RT 0.39 - 0.91 (30 scans) - Background Subtracted 0.20 - 0.38
mtc-1-270125_Scan1_1s1.dab;
APCI+ Max: 2E8

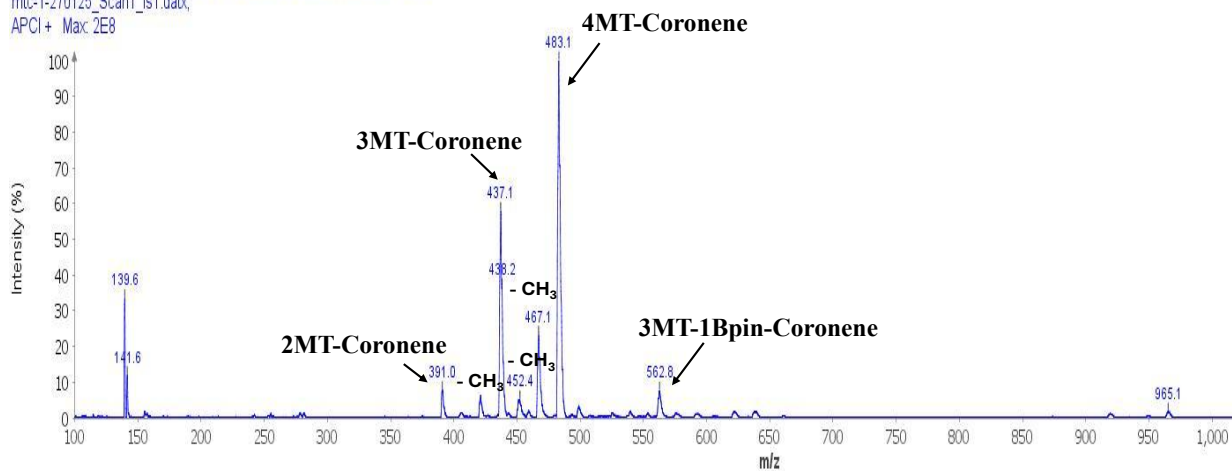


Fig. S30. APCI-MS spectra (not high resolution) of the crude product containing MT-coronene before sublimation.

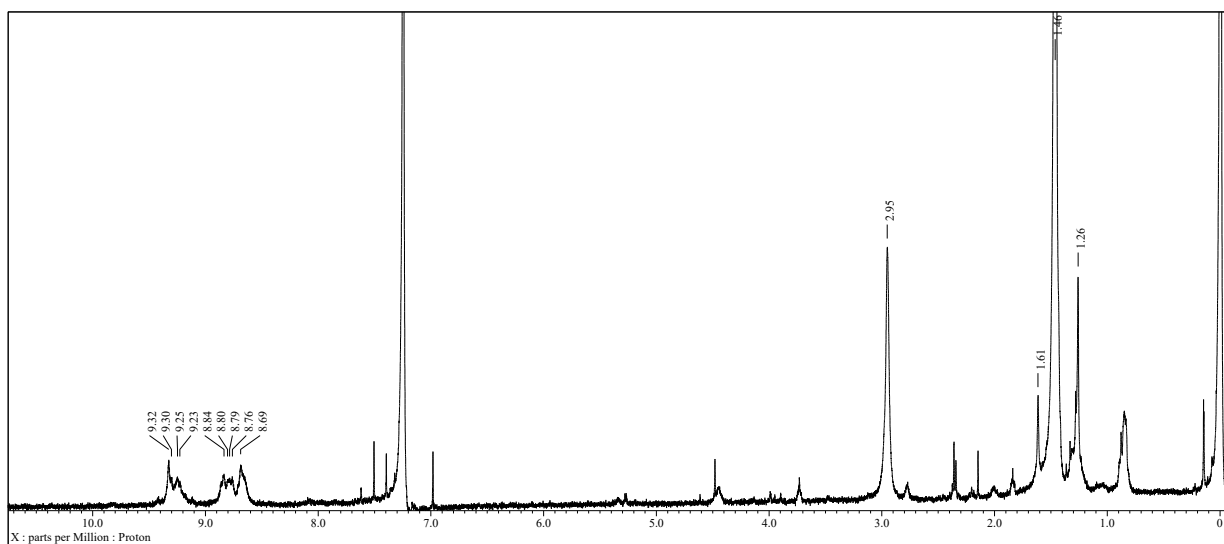


Fig. S31. ¹H NMR spectra of the crude product (in CDCl₃ at 50 °C) before sublimation.

14. References

1. K. Bulgarevich, S. Horiuchi and K. Takimiya, *Adv. Mater.*, 2023, **35**, 2305548.
2. K. Bulgarevich and K. Takimiya, *Mater. Horiz.*, 2023, **10**, 5492-5499.
3. M. J. Frisch, G. W. Trucks, H. B. Schlegel, G. E. Scuseria, M. A. Robb, J. R. Cheeseman, G. Scalmani, V. Barone, G. A. Petersson, H. Nakatsuji, X. Li, M. Caricato, A. V. Marenich, J. Bloino, B. G. Janesko, R. Gomperts, B. Mennucci, H. P. Hratchian, J. V. Ortiz, A. F. Izmaylov, J. L. Sonnenberg, D. Williams-Young, F. Ding, F. Lipparini, F. Egidi, J. Goings, B. Peng, A. Petrone, T. Henderson, D. Ranasinghe, V. G. Zakrzewski, J. Gao, N. Rega, G. Zheng, W. Liang, M. Hada, M. Ehara, K. Toyota, R. Fukuda, J. Hasegawa, M. Ishida, T. Nakajima, Y. Honda, O. Kitao, H. Nakai, T. Vreven, K. Throssell, J. A. Montgomery Jr., J. E. Peralta, F. Ogliaro, M. J. Bearpark, J. J. Heyd, E. N. Brothers, K. N. Kudin, V. N. Staroverov, T. A. Keith, R. Kobayashi, J. Normand, K. Raghavachari, A. P. Rendell, J. C. Burant, S. S. Iyengar, J. Tomasi, M. Cossi, J. M. Millam, M. Klene, C. Adamo, R. Cammi, J. W. Ochterski, R. L. Martin, K. Morokuma, O. Farkas, J. B. Foresman and D. J. Fox, *Journal*, 2016.
4. M. N. Eliseeva and L. T. Scott, *J. Am. Chem. Soc.*, 2012, **134**, 15169-15172.
5. S. Yoshida, Y. Sugimura, Y. Hazama, Y. Nishiyama, T. Yano, S. Shimizu and T. Hosoya, *Chem. Commun.*, 2015, **51**, 16613-16616.
6. K. Kanemoto, S. Yoshida and T. Hosoya, *Chem. Lett.*, 2017, **47**, 85-88.
7. K. Takimiya, K. Bulgarevich and S. Horiuchi, *J. Mater. Chem. C*, 2023, **11**, 10809-10815.
8. R. Yamaguchi, S. Ito, B. S. Lee, S. Hiroto, D. Kim and H. Shinokubo, *Chem. - Asian J.*, 2013, **8**, 178-190.
9. A. M. Moussa, J.-R. Yang and M. E. Langmuir, *Org. Prep. Proced. Int.*, 1993, **25**, 252-255.
10. T. Mukaiyama, T. Sato and J. Hanna, *Chem. Lett.*, 1973, **2**, 1041-1044.
11. F. B. Mallory and C. W. Mallory, *Organic Reactions*, John Wiley and Sons, 1984.
12. S. Alibert-Fouet, I. Seguy, J.-F. Bobo, P. Destruel and H. Bock, *Chem. Eur. J.*, 2007, **13**, 1746-1753.
13. C.-H. Chiang, D. Pangeni and E. E. Nesterov, *Macromolecules*, 2017, **50**, 6961-6966.
14. G. Sheldrick, *Acta Crystallogr. Sec. A*, 2015, **71**, 3-8.
15. G. Sheldrick, *Acta Crystallogr. Sec. C*, 2015, **71**, 3-8.
16. O. V. Dolomanov, L. J. Bourhis, R. J. Gildea, J. A. K. Howard and H. Puschmann, *J. Appl. Crystallogr.*, 2009, **42**, 339-341.
17. G. R. Desiraju and A. Gavezzotti, *Acta Crystallogr. Sec. B*, 1989, **45**, 473-482.
18. K. Takimiya, K. Bulgarevich and K. Kawabata, *Acc. Chem. Res.*, 2024, **57**, 884-894.
19. J. Shin, K. Bulgarevich and K. Takimiya, *Cryst. Growth Des.*, 2025, **25**, 687-693.
20. M. Berblinger and C. Schlier, *Comput. Phys. Commun.*, 1991, **66**, 157-166.